



Waves and instabilities of viscoelastic fluid film flowing down an inclined wavy bottomSanghasri Mukhopadhyay ^{1,*} and Asim Mukhopadhyay ²¹*Laboratoire LOCIE, Université Savoie Mont Blanc, Chambéry 73000, France*²*Vivekananda Mahavidyalaya, Burdwan 713103, West Bengal, India*

(Received 3 July 2020; accepted 14 August 2020; published 31 August 2020)

Evolution of waves and hydrodynamic instabilities of a thin viscoelastic fluid film flowing down an inclined wavy bottom of moderate steepness have been analyzed analytically and numerically. The classical long-wave expansion method has been used to formulate a nonlinear evolution equation for the development of the free surface. A normal-mode approach has been adopted to discuss the linear stability analysis from the viewpoint of the spatial and temporal study. The method of multiple scales is used to derive a Ginzburg-Landau-type nonlinear equation for studying the weakly nonlinear stability solutions. Two significant wave families, *viz.*, γ_1 and γ_2 , are found and discussed in detail along with the traveling wave solution of the evolution system. A time-dependent numerical study is performed with Scikit-FDif. The entire investigation is conducted primarily for a general periodic bottom, and the detailed results of a particular case study of sinusoidal topography are then discussed. The case study reveals that the bottom steepness ζ plays a dual role in the linear regime. Increasing ζ has a stabilizing effect in the uphill region, and the opposite occurs in the downhill region. While the viscoelastic parameter Γ has a destabilizing effect throughout the domain in both the linear and the nonlinear regime. Both supercritical and subcritical solutions are possible through a weakly nonlinear analysis. It is interesting to note that the unconditional zone decreases and the explosive zone increases in the downhill region rather than the uphill region for a fixed Γ and ζ . The same phenomena occur in a particular region if we increase Γ and keep ζ fixed. The traveling wave solution reveals the fact that to get the γ_1 family of waves we need to increase the Reynolds number a bit more than the value at which the γ_2 family of waves is found. The spatiotemporal evolution of the nonlinear surface equation indicates that different kinds of finite-amplitude permanent waves exist.

DOI: [10.1103/PhysRevE.102.023117](https://doi.org/10.1103/PhysRevE.102.023117)**I. INTRODUCTION**

Investigations of thin liquid films are one of the most important hydrodynamic problems, as they are ubiquitous in nature and technology; this has attracted much attention from a number of researchers over the last six decades. A simple and obvious example is the flow of rainwater down a windowpane under the action of gravity. It has extensive use in various industrial and technological applications such as evaporators, condensers, heat exchangers [1,2], canisters for nuclear waste disposal, nuclear reactor cooling systems, material processing, food and chemical industries, biomedical engineering, and geothermal reservoirs. A typical thin-film flow consists of an expanse of a liquid partially bounded by solid substrates with an interface where the liquid is exposed to another fluid, usually gas and most often air in applications. The solid substrates may be planar or undulated. It is well known that the waves on the surface of a thin film enhance the transport of heat mass and momentum across the liquid-gas and liquid-solid interface. In some applications, the presence of surface waves may be a desirable feature, as in the case of cooling films, where they enhance heat and mass transfer [3,4]. On the other hand, it is undesirable in the coating films

to increase the glossy texture of the finished product [5]. So to model improved devices, it is desirable to know details about the film flow and its finite-amplitude behavior.

Wave evolution on falling liquid film has been extensively studied over the last few decades, starting from the pioneering work by Kapitza [6] and Kapitza and Kapitza [7], in which a vast variety of wavy regimes, like a rolling wave with a capillary hill and a series of nearly solitary waves or almost-harmonic waves of falling liquid films, was observed. In this situation, we need to understand the stability and its criteria for falling films. In 1957 Benjamin [8] and in 1963 Yih [9] were reportedly the first to investigate theoretically the long-wave instability of falling film over an inclined plane. They determined the phase velocity of the waves and critical Reynolds number for the transition, respectively. In 1966 Benney [10] derived a wave evolution equation governing the flow by regular perturbation technique in terms of flow depth, by expanding the variables in powers of the long-wave parameter. Extensive reviews of the literature for the film flow over flat inclined or vertical substrates with various effects are reported by Fulford [11], Hanratty [12], Chang and Demekhin [12], Lin and Wang [13], and Chang [14].

The corresponding problem of falling film for non-Newtonian fluid has also been studied extensively, since the simple model of considering the linear law of viscous fluids is not a reasonable approximation to the real physical

*sanghasri.mukhopadhyay@univ-smb.fr

situation. For many real fluids, the resistance of the flow changes with the intensity of the shear rate. This change of viscosity can be large and cannot be ignored in such fluids. There are many approaches that deviate from Newtonian to non-Newtonian that exhibit some or many aspects of the real physical situation. Some of these fluids exhibit shear thinning or thickening, while some others possess elastic properties or something else. There are many examples of fluids which possess the characteristic of elastic properties and so-called cross-viscosity. When such a fluid is in motion, the flow energy is partially reserved as strain energy and partially incorporated by internal viscous forces and dissipated as heat to the environment; these types of fluids are known as viscoelastic fluids. The elastic properties of these types of fluids can create shear on an element of the fluid to be regressed, and the elastic stresses cannot be relaxed at a certain frequency as the flow moves down a vertical wall. There are various models suggested in the literature to describe viscoelastic fluids, such as the second-order model, the Oldroyd B model, and Walters' B'' model. The rheological behavior of the fluids characterized by each and every model is completely different, and almost every one has some limitations, but almost every one satisfactorily describes a particular type of fluid. For example, the second-order fluid model describes very successfully fluids with gradually fading memory, while Walters' B'' fluid model is valid for short or rapidly fading memory liquids (weakly elastic) where the resulting flow should be considered a perturbation of Newtonian viscous flow [15]. To get some perception of the flow behavior of viscoelastic fluids, it is preferable to restrict oneself to a model with a minimum number of parameters in the constitutive equations. We chose Walters' B'' [16] viscoelastic fluid model for our study, as it requires only one non-Newtonian parameter.

Since the trailblazing work by Gupta [17] in 1967 many researchers have carried out their work on falling films by considering different models of viscoelastic fluids to investigate waves and instabilities over a flat surface [18–23]. Most relevant to this present work, Cheng *et al.* [24] conducted a stability analysis of thin viscoelastic Walters' B'' fluid flowing down a vertical wall by using the long-wave perturbation method. Recently, Uma and Usha [25] investigated linearized instability for permanent waves on a thin viscoelastic Walters' B'' fluid layer flowing down an inclined plane. They also categorized the eigenvalue properties of the fixed points in various parametric regimes.

Nonetheless, the above studies are focused only on the film flows down flat inclined or vertical substrates, but in most of the applications, the film does not flow over a perfectly flat substrate. During the last few decades, a lot of advancements have been made in the use of renewable energy, for example, solar energy, wind energy, and waste heat from industrial wastage. For solar energy, utilized in solar refrigeration, solar heat storage, and transportation of heat or cooling over a large distance, the process of absorption or desorption is widely used. In most cases, the apparatus is built purposefully with a wavy surface, while in other applications corrugation simply cannot be avoided. Thus, in either case, it is of interest to us to investigate how the alterations from the ideal condition of a flat incline affect the gravity-driven film flow with various physical effects. Tougou [26] investigated theoretically the

influence of a weakly wavy bottom on the stability of steady film flow. The hydrodynamics of a liquid film falling down an undulated surface has gained a lot of attention since the work of Pozrikidis [27], who studied the free surface Stokes flow along with the sinusoidal topography. Later, Wierschem *et al.* [28] studied experimentally the linear stability of film flow over modulations of moderate steepness, which has long been compared to the film thickness. They found that the critical Reynolds number for the onset of surface waves is higher than that for a flat bottom. Investigation of a viscous film flowing down a harmonic vertical substrate was done by Trifonov [29,30]. He contemplated the effect of surface tension, viscosity, and inertia. Mogilevskiy and Shkadov [31] used the integral boundary layer approach to model the problem of a thin film flow on a weakly wavy wall. They showed that, depending on the corrugation period and the inclination angle of the plane, the topography can both stabilize and destabilize the flow. Veremieiev and Wacks [32] developed an extension of the weighted residual model proposed by Ruyer-Quil and Manneville [33] and D'alesio *et al.* [34] and included third and fourth terms in the long-wavelength expansion to enlarge the new modeling strategy for flow on an inclined corrugated substrate.

Other research work, by Vlachogiannis and Bontozoglou [35], Wierschem and Aksel [36], Wierschem *et al.* [37], Davalos-Orozco [38], Häcker and Uecker [39], Heining and Aksel [40], Pollak and Aksel [41], Trifonov [42], etc., is also dedicated to the study of the effect of bottom topography in the flow of falling films for several physical problems. An excellent review of the film flow over different topographies is given by Aksel and Schörner [43].

In 2010 a remarkable work on power-law fluid flowing down a wavy incline was done by Heining and Aksel [44], who investigated the effects of inertia and surface tension on bottom undulation. They found a resonant interaction of the free surface with the wavy bottom under the assumption of periodic undulation with weak steepness and concluded that “high surface tension requires [a] higher Reynolds number to achieve resonance.” Prior to that, Wierschem *et al.* [45] and Heining *et al.* [46] explained in detail the surface amplification phenomenon (called resonance in the literature) for viscous film on an inclined wavy bottom.

In the present study, we present an analysis of finite-amplitude long-wave instabilities and the evolution of a thin viscoelastic film falling down over inclined generalized periodic wavy bottoms. The flow over a wavy bottom may change the dominant mode of instability due to the viscoelastic property of the fluid. As far as we are aware, the evolution of waves and hydrodynamic instabilities of a viscoelastic film falling through a general undulated surface has not been studied intensively so far. Our study will help to explore a broader gateway to handle many industrial and natural phenomena.

II. PROBLEM FORMULATION

Let us consider a thin viscoelastic fluid, represented by Walters' B'' , a fluid film of density ρ , dynamic viscosity μ , and surface tension s_0 flowing down an incline wavy bottom profile \hat{b} . The fluid is assumed to be non-Newtonian. The Cartesian coordinate system $\mathbf{e}_x, \mathbf{e}_y$ is inclined at an angle β

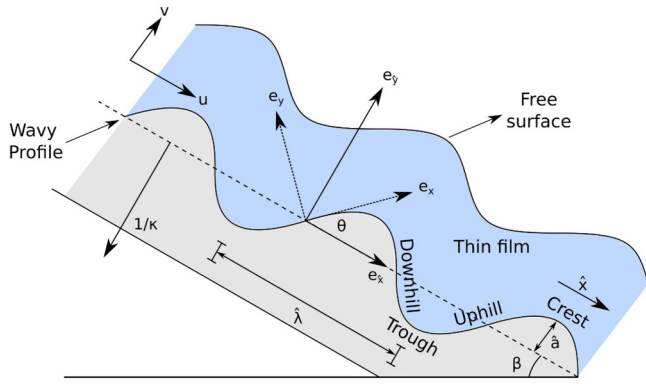


FIG. 1. Diagrammatic picture.

with respect to the horizontal, and the bottom profile $\hat{b}(\hat{x})$ is periodic with wavelength $\hat{\lambda}$ and amplitude \hat{a} , where \hat{x} is in the direction of the main flow. For an undulated bottom profile it is useful and appropriate to introduce a local curvilinear coordinate system, since the Nusselt solution is no longer a stationary solution, and for the flow of thin films that are thinner than the radius of curvature of the bottom, the flow (u, v) is still mainly parallel to the bottom (see Fig. 1). Thus, at every point of the bottom $\hat{x}\mathbf{e}_{\hat{x}} + \hat{b}(\hat{x})\mathbf{e}_{\hat{y}}$ we define a local coordinate system $\mathbf{e}_x, \mathbf{e}_y$, with \mathbf{e}_x tangential and \mathbf{e}_y normal to the bottom. Thus, for an arbitrary point P within the fluid, the arc length x of the bottom and the distance y along \mathbf{e}_y to the bottom are now taken as curvilinear coordinates. So in $\mathbf{e}_{\hat{x}}, \mathbf{e}_{\hat{y}}$ coordinates $P \equiv (\hat{x} - \sin\theta y, \hat{b}(\hat{x}) + \cos\theta y)$, where $\theta = \theta(\hat{x}) = \arctan(\partial\hat{b}(\hat{x})/\partial\hat{x})$ is the local inclination angle between $\mathbf{e}_{\hat{x}}$ and \mathbf{e}_x . This relation is always unique, as we considered the film flow over undulated bottoms of moderate steepness, which have long been compared to the film thickness. To transform gradients, we also need the bottom curvature κ , which is defined by

$$\kappa(\hat{x}) = -\frac{\partial^2\hat{b}(\hat{x})}{\partial\hat{x}^2} \left[1 + \left(\frac{\partial\hat{b}(\hat{x})}{\partial\hat{x}} \right)^2 \right]^{-3/2}. \quad (1)$$

For further details regarding the transformation to curvilinear coordinates, we refer to Wierschem *et al.* [28].

A. Governing equation

The governing equations consist of the conservation of mass and momentum. In dimensional form they can be written as

$$\nabla \cdot \mathbf{V} = 0, \quad (2)$$

$$\rho \frac{D\mathbf{V}}{Dt} = \rho\mathbf{g} + \nabla \cdot \boldsymbol{\tau}, \quad (3)$$

where $\nabla = \frac{1}{1+\kappa y}\mathbf{e}_{\hat{x}}\frac{\partial}{\partial x} + \mathbf{e}_{\hat{y}}\frac{\partial}{\partial y}$, $\vec{V} = u\mathbf{e}_{\hat{x}} + v\mathbf{e}_{\hat{y}}$, and $\frac{D}{Dt} \equiv \frac{\partial}{\partial t} + \mathbf{V} \cdot \nabla$ is the material derivative. \mathbf{g} is the acceleration due to gravity. The Cauchy stress tensor $\boldsymbol{\tau}$ is given by Beard and Walters [16] as

$$\boldsymbol{\tau} = -p\mathbf{I} + 2\mu\boldsymbol{\sigma} - 2\gamma_0\frac{\delta\boldsymbol{\sigma}}{\delta t}, \quad (4)$$

where p is the isotropic pressure, μ is the dynamic viscosity of the fluid at low rates of shear, and γ_0 is the short memory coefficient or viselastic coefficient of the fluid. The rate of strain tensor $\boldsymbol{\sigma}$ is defined by $\boldsymbol{\sigma} = (\nabla\mathbf{V} + \nabla\mathbf{V}^T)/2$ and $\frac{\delta}{\delta t}$ denotes the convected (or Oldroyd) derivative given by

$$\frac{\delta\boldsymbol{\sigma}}{\delta t} = \frac{\partial\boldsymbol{\sigma}}{\partial t} + \mathbf{V} \cdot \nabla\boldsymbol{\sigma} - \boldsymbol{\sigma} \cdot \nabla\mathbf{V} - (\nabla\mathbf{V})^T \cdot \boldsymbol{\sigma}. \quad (5)$$

The pertinent boundary conditions include the usual no-slip condition at the bottom:

$$\mathbf{V} = 0 \quad \text{at } y = 0. \quad (6)$$

At the free surface, $y = h(x, t)$ dynamic and kinematic conditions are

$$\mathbf{n} \cdot \boldsymbol{\tau} \cdot \mathbf{t} = 0, \quad (7)$$

$$p_a + \mathbf{n} \cdot \boldsymbol{\tau} \cdot \mathbf{n} = -s_0\nabla \cdot \mathbf{n}, \quad (8)$$

$$h_t + \mathbf{V} \cdot \nabla(h - y) = 0, \quad (9)$$

where p_a is the pressure of the ambient gas and s_0 is the surface tension coefficient.

$$\mathbf{n} = \frac{\mathbf{e}_y - \frac{1}{1+\kappa h}h_x\mathbf{e}_x}{\sqrt{1 + \left(\frac{1}{1+\kappa h}h_x\right)^2}}, \quad \mathbf{t} = \frac{\mathbf{e}_x + \frac{1}{1+\kappa h}h_x\mathbf{e}_y}{\sqrt{1 + \left(\frac{1}{1+\kappa h}h_x\right)^2}}$$

are the normal and tangential unit vectors pointing outwards to the interface, respectively.

To investigate the effect of waviness of the bottom on the flow we use the thin film flow over a flat bottom as reference. Thus, the Nusselt velocity of the mean flow $\langle u \rangle = g \sin\beta \hat{h}^2/3\nu$, where $\nu = \mu/\rho$ is the kinematic viscosity and \hat{h} is the constant film thickness, is taken as the characteristic velocity and $\hat{\lambda}$ as the characteristic longitudinal length scale, whose order may be considered the same as the wavelength of the free surface wave, which is very long compared to the film thickness.

B. Scaling and nondimensionalization

Before solving the problem, we want to rewrite it precisely in dimensionless format. We define the dimensionless quantities as

$$x^* = \frac{2\pi}{\hat{\lambda}}x, \quad y^* = \frac{1}{\hat{h}}y, \quad h^* = \frac{1}{\hat{h}}h, \quad u^* = \frac{1}{\langle u \rangle}u,$$

$$v^* = \frac{\hat{\lambda}}{2\pi\hat{h}\langle u \rangle}v, \quad t^* = \frac{2\pi\langle u \rangle}{\hat{\lambda}}t, \quad \kappa^* = \frac{\hat{\lambda}^2}{4\pi^2\hat{a}}\kappa,$$

$$p^* = \frac{1}{\rho\langle u \rangle^2}p, \quad (\tau_{xx}^*, \tau_{yy}^*) = \frac{\lambda}{2\pi\mu\langle u \rangle}(\tau_{xx}, \tau_{yy}),$$

$$\hat{x}^*(x^*) = \frac{2\pi}{\hat{\lambda}}\hat{x}(x), \quad (\tau_{xy}^*, \tau_{yx}^*) = \frac{\hat{h}}{\mu\langle u \rangle}(\tau_{xy}, \tau_{yx}),$$

$$\hat{b}^*(x^*) = \frac{1}{\hat{a}}\hat{b}\left(\frac{\hat{\lambda}}{2\pi}x^*\right), \quad \theta^* = \arctan\left(\zeta\frac{\partial\hat{b}^*}{\partial\hat{x}^*}\right), \quad (10)$$

where $\zeta = 2\pi\hat{a}/\hat{\lambda}$ is the bottom steepness and $\varepsilon = 2\pi\hat{h}/\hat{\lambda}$ is the aspect ratio.

Using the dimensionless quantities, (10), in the governing equations, (2)–(9), we arrive, after dropping the asterisk, at

$$\frac{1}{1 + \varepsilon\zeta\kappa y} \left(\frac{\partial u}{\partial x} + \varepsilon\zeta\kappa v \right) + \frac{\partial v}{\partial y} = 0, \tag{11}$$

$$\begin{aligned} \varepsilon \text{Re} \left[\frac{\partial u}{\partial t} + \frac{1}{1 + \varepsilon\zeta\kappa y} u \left(\frac{\partial u}{\partial x} + \varepsilon\zeta\kappa v \right) + v \frac{\partial u}{\partial y} \right] \\ = 3SS + \left[\frac{\varepsilon^2}{1 + \varepsilon\zeta\kappa y} \frac{\partial \tau_{xx}}{\partial x} + \frac{\partial \tau_{xy}}{\partial y} + \frac{2\varepsilon\zeta\kappa}{1 + \varepsilon\zeta\kappa y} \tau_{xy} \right], \tag{12} \end{aligned}$$

$$\begin{aligned} \varepsilon^2 \text{Re} \left[\frac{\partial v}{\partial t} + \frac{1}{1 + \varepsilon\zeta\kappa y} u \left(\frac{\partial v}{\partial x} - \frac{1}{\varepsilon} \zeta\kappa u \right) + v \frac{\partial v}{\partial y} \right] \\ = -3CS + \varepsilon \left[\frac{1}{1 + \varepsilon\zeta\kappa y} \frac{\partial \tau_{yx}}{\partial x} + \frac{\partial \tau_{yy}}{\partial y} \right. \\ \left. + \frac{\varepsilon\zeta\kappa}{1 + \varepsilon\zeta\kappa y} (\tau_{yy} - \tau_{xx}) \right], \tag{13} \end{aligned}$$

where $SS = \frac{\sin(\beta-\theta)}{\sin\beta}$ and $CS = \frac{\cos(\beta-\theta)}{\sin\beta}$,

$$u = 0, \quad v = 0 \quad \text{at} \quad y = 0. \tag{14}$$

At the free surface $y = h(x, t)$,

$$(1 - \varepsilon^2 h_x^2) \tau_{yx} + \varepsilon^2 (\tau_{yy} - \tau_{xx}) h_x = 0, \tag{15}$$

$$\begin{aligned} p_a + \frac{\varepsilon}{\text{Re}} \left[\varepsilon^2 \tau_{xx} h_x^2 - 2\tau_{yx} h_x + \tau_{yy} \right] \\ = \varepsilon^2 \text{We} (h_{xx} - \zeta \varepsilon^{-1} \kappa + 2\zeta^2 \kappa^2 h) (1 + \varepsilon^2 h_x^2)^{-\frac{1}{2}}, \tag{16} \end{aligned}$$

$$h_t + \frac{1}{1 + \varepsilon\zeta\kappa h} u h_x = v. \tag{17}$$

In the dimensionless form the component of stress tensor given in (4) can be written as

$$\begin{aligned} \tau_{xx} = \left[-\frac{\text{Re}}{\varepsilon} p + \frac{2}{1 + \varepsilon\zeta\kappa y} \left(\frac{\partial u}{\partial x} + \varepsilon\zeta\kappa v \right) \right] \\ - 2\varepsilon \text{Re} \Gamma \left[\frac{1}{1 + \varepsilon\zeta\kappa y} \frac{\partial}{\partial t} \left(\frac{\partial u}{\partial x} + \varepsilon\zeta\kappa v \right) \right. \\ \left. + \left(\frac{1}{1 + \varepsilon\zeta\kappa y} u \frac{\partial}{\partial x} + v \frac{\partial}{\partial y} \right) \right. \\ \left. \times \left\{ \frac{1}{1 + \varepsilon\zeta\kappa y} \left(\frac{\partial u}{\partial x} + \varepsilon\zeta\kappa v \right) \right\} \right. \\ \left. - \frac{2}{(1 + \varepsilon\zeta\kappa y)^2} \left(\frac{\partial u}{\partial x} + \varepsilon\zeta\kappa v \right)^2 - \frac{1}{\varepsilon^2} \frac{\partial u}{\partial y} \right. \\ \left. \times \left\{ \frac{1}{1 + \varepsilon\zeta\kappa y} \left(\varepsilon^2 \frac{\partial v}{\partial x} - \varepsilon\zeta\kappa u \right) + \frac{\partial u}{\partial y} \right\} \right], \tag{18} \end{aligned}$$

$$\begin{aligned} \tau_{xy} = \tau_{yx} = \left[\frac{1}{1 + \varepsilon\zeta\kappa y} \left(\varepsilon^2 \frac{\partial v}{\partial x} - \varepsilon\zeta\kappa u \right) + \frac{\partial u}{\partial y} \right] \\ - \varepsilon \text{Re} \Gamma \left[\frac{\partial}{\partial t} \left\{ \frac{1}{1 + \varepsilon\zeta\kappa y} \left(\varepsilon^2 \frac{\partial v}{\partial x} - \varepsilon\zeta\kappa u \right) + \frac{\partial u}{\partial y} \right\} \right. \\ \left. + \left(\frac{1}{1 + \varepsilon\zeta\kappa y} u \frac{\partial}{\partial x} + v \frac{\partial}{\partial y} \right) \right. \\ \left. \times \left\{ \frac{1}{1 + \varepsilon\zeta\kappa y} \left(\varepsilon^2 \frac{\partial v}{\partial x} - \varepsilon\zeta\kappa u \right) + \frac{\partial u}{\partial y} \right\} \right] \end{aligned}$$

$$\begin{aligned} - \frac{2}{(1 + \varepsilon\zeta\kappa y)^2} \left(\varepsilon^2 \frac{\partial v}{\partial x} - \varepsilon\zeta\kappa u \right) \\ \times \left(\frac{\partial u}{\partial x} + \varepsilon\zeta\kappa v \right) - 2 \frac{\partial v}{\partial y} \frac{\partial u}{\partial y} \right], \tag{19} \end{aligned}$$

$$\begin{aligned} \tau_{yy} = \left[-\frac{\text{Re}}{\varepsilon} p + 2 \frac{\partial v}{\partial y} \right] - 2\varepsilon \text{Re} \Gamma \left[\frac{\partial^2 v}{\partial t \partial y} + \frac{1}{1 + \varepsilon\zeta\kappa y} \right. \\ \left. \times \left(u \frac{\partial^2 v}{\partial x \partial y} + v \frac{\partial^2 v}{\partial y^2} \right) - \frac{1}{\varepsilon^2} \frac{1}{1 + \varepsilon\zeta\kappa y} \left(\varepsilon^2 \frac{\partial v}{\partial x} - \varepsilon\zeta\kappa u \right) \right. \\ \left. \times \left\{ 1 + \varepsilon\zeta\kappa y \left(\varepsilon^2 \frac{\partial v}{\partial x} - \varepsilon\zeta\kappa u \right) + \frac{\partial u}{\partial y} \right\} - 2 \left(\frac{\partial v}{\partial y} \right)^2 \right], \tag{20} \end{aligned}$$

where $\text{Re} (\equiv \langle u \rangle \hat{h} / \nu)$ is the *Reynolds number*, which is of $O(1)$, $\text{We} (\equiv s_0 / \rho \langle u \rangle^2 \hat{h})$ is the *Weber number*, which is of $O(1/\varepsilon^2)$, and $\Gamma (\equiv \gamma_0 / \rho \hat{h}^2)$ is the viscoelastic parameter $O(1)$. Also, it is assumed that the order of ζ is 1 or smaller with the thin-film parameter ε .

Using Eqs. (18)–(20) in Eqs. (11)–(17) and retaining the terms up to $O(\varepsilon)$ we have the following.

1. Reduced governing equations

$$\frac{\partial u}{\partial x} + \frac{\partial v}{\partial y} + \varepsilon\zeta\kappa \left(v + y \frac{\partial v}{\partial y} \right) = 0, \tag{21}$$

$$\begin{aligned} \varepsilon \text{Re} \left(\frac{\partial u}{\partial t} + u \frac{\partial u}{\partial x} + v \frac{\partial u}{\partial y} \right) \\ = -\varepsilon \text{Re} \frac{\partial p}{\partial x} + 3SS + \frac{\partial^2 u}{\partial y^2} \\ + \varepsilon\kappa\zeta \frac{\partial u}{\partial y} - \varepsilon \text{Re} \Gamma \left[\frac{\partial^3 u}{\partial t \partial y^2} + u \frac{\partial^3 u}{\partial x \partial y^2} + v \frac{\partial^3 u}{\partial y^3} \right. \\ \left. + \frac{\partial u}{\partial x} \frac{\partial^2 u}{\partial y^2} - \frac{\partial u}{\partial y} \frac{\partial^2 u}{\partial x \partial y} \right] + O(\varepsilon^2), \tag{22} \end{aligned}$$

$$-\varepsilon \text{Re} \zeta \kappa u^2 = -\text{Re} \frac{\partial p}{\partial y} - 3CS + \varepsilon \frac{\partial^2 v}{\partial y^2} + O(\varepsilon^2). \tag{23}$$

2. Reduced boundary conditions

$$u = 0, \quad v = 0 \quad \text{at} \quad y = 0, \tag{24}$$

$$\begin{aligned} \frac{\partial u}{\partial y} + \varepsilon\zeta\kappa \left(2h \frac{\partial u}{\partial y} - u \right) \\ = \varepsilon \text{Re} \Gamma \left[\frac{\partial^2 u}{\partial t \partial y} + u \frac{\partial^2 u}{\partial x \partial y} + v \frac{\partial^2 u}{\partial y^2} - 2 \frac{\partial u}{\partial y} \frac{\partial v}{\partial y} \right. \\ \left. + 2 \left(\frac{\partial u}{\partial y} \right)^2 h_x \right] + O(\varepsilon^2), \tag{25} \end{aligned}$$

$$\begin{aligned} p = p_a + \frac{2\varepsilon}{\text{Re}} \left(\frac{\partial v}{\partial y} + \frac{\partial u}{\partial y} h_x \right) - \varepsilon^2 \text{We} (h_{xx} - \zeta \varepsilon^{-1} \kappa \\ + 2\zeta^2 \kappa^2 h) + O(\varepsilon^2), \tag{26} \end{aligned}$$

$$\frac{\partial h}{\partial t} + u \frac{\partial h}{\partial x} - v - \varepsilon\zeta\kappa h u \frac{\partial h}{\partial x} + O(\varepsilon^2) = 0. \tag{27}$$

III. LONG-WAVE APPROXIMATION

We are interested in constructing a nonlinear evolution equation in terms of a nondimensional film thickness $h(x, t)$, depending on the dimensionless spatial and temporal variables x and t . Expanding the physical quantities u , v , and p as a power series of the long-wave parameter ε ,

$$\begin{aligned} u &= u_0 + \varepsilon u_1 + \dots, \\ v &= v_0 + \varepsilon v_1 + \dots, \\ p &= p_0 + \varepsilon p_1 + \dots, \end{aligned} \tag{28}$$

and substituting the above into the governing equations (21)–(23) and the boundary conditions (24)–(27) and then collecting the coefficients of like powers of ε , the zeroth- and the first-order equations are obtained as reported below.

1. Zeroth-order equations

$$\frac{\partial u_0}{\partial x} + \frac{\partial v_0}{\partial y} = 0, \tag{29}$$

$$3SS + \frac{\partial^2 u_0}{\partial y^2} = 0, \tag{30}$$

$$-\text{Re} \frac{\partial p_0}{\partial y} - 3CS = 0. \tag{31}$$

At $y = 0$

$$u_0 = 0, \quad v_0 = 0. \tag{32}$$

At $y = h$

$$\frac{\partial h}{\partial t} + u_0 \frac{\partial h}{\partial x} = v_0, \tag{33}$$

$$\frac{\partial u_0}{\partial y} = 0, \tag{34}$$

$$p_0 = p_a - \varepsilon^2 \text{We}(h_{xx} - \zeta \varepsilon^{-1} \kappa + 2\zeta^2 \kappa^2 h). \tag{35}$$

2. First-order equations

$$\frac{\partial u_1}{\partial x} + \frac{\partial v_1}{\partial y} + \zeta \kappa v_0 + \zeta \kappa y \frac{\partial v_0}{\partial y} = 0, \tag{36}$$

$$\begin{aligned} &\text{Re} \left(\frac{\partial u_0}{\partial t} + u_0 \frac{\partial u_0}{\partial x} + v_0 \frac{\partial u_0}{\partial y} \right) \\ &= -\text{Re} \frac{\partial p_0}{\partial x} + \zeta \kappa \frac{\partial u_0}{\partial y} + \frac{\partial^2 u_1}{\partial y^2} - \text{Re} \Gamma \left[\frac{\partial^3 u_0}{\partial t \partial y^2} \right. \\ &\quad \left. + u_0 \frac{\partial^3 u_0}{\partial x \partial y^2} + v_0 \frac{\partial^3 u_0}{\partial y^3} + \frac{\partial u_0}{\partial x} \frac{\partial^2 u_0}{\partial y^2} - \frac{\partial u_0}{\partial y} \frac{\partial^2 u_0}{\partial x \partial y} \right], \end{aligned} \tag{37}$$

$$-\text{Re} \zeta \kappa u_0^2 = -\text{Re} \frac{\partial p_1}{\partial y} + \frac{\partial^2 v_0}{\partial y^2}. \tag{38}$$

At $y = 0$

$$u_1 = 0, \quad v_1 = 0, \tag{39}$$

At $y = h$

$$u_1 \frac{\partial h}{\partial x} - v_1 - \zeta \kappa h u_0 \frac{\partial h}{\partial x} = 0, \tag{40}$$

$$\begin{aligned} \frac{\partial u_1}{\partial y} + \zeta \kappa \left(2h \frac{\partial u_0}{\partial y} - u_0 \right) &= \text{Re} \Gamma \left[\frac{\partial^2 u_0}{\partial t \partial y} + u_0 \frac{\partial^2 u_0}{\partial x \partial y} v_0 \frac{\partial^2 u_0}{\partial y^2} \right. \\ &\quad \left. + 2 \frac{\partial u_0}{\partial x} \frac{\partial u_0}{\partial y} + 2 \left(\frac{\partial u_0}{\partial y} \right)^2 \frac{\partial h}{\partial x} \right], \end{aligned} \tag{41}$$

$$p_1 = \frac{2}{\text{Re}} \left(\frac{\partial v_0}{\partial y} + \frac{\partial u_0}{\partial y} \frac{\partial h}{\partial x} \right). \tag{42}$$

Now solving Eqs. (29)–(42) we obtain the zeroth- and first-order velocities and corresponding depth average velocities as reported below.

3. Zeroth-order solutions

$$u_0 = -3SS \left(\frac{1}{2} y^2 - hy \right), \tag{43}$$

$$v_0 = -3SS \frac{y^2}{2} h_x, \tag{44}$$

$$p_0 = p_a - \frac{3}{\text{Re}} CS(y - h) - \varepsilon^2 \text{We}(h_{xx} - \zeta \varepsilon^{-1} \kappa + 2\zeta^2 \kappa^2 h), \tag{45}$$

$$q_0 = \int_0^h u_0 dy = SS h^3. \tag{46}$$

4. First-order solutions

$$\begin{aligned} u_1 &= \frac{1}{2} \text{Re} SS (y^3 - 3yh^2) h_t + \frac{3}{8} \text{Re} SS^2 [(y^3 - 4h^3) hy] h_x \\ &\quad - \frac{3}{2} \Gamma \text{Re} SS y [-2h_t + 3SSh(y - 4h) h_x] \\ &\quad + \text{Re} \left(\frac{y^2}{2} - hy \right) \left[\frac{3CS}{\text{Re}} h_x - \varepsilon^2 \text{We} \left(h_{xxx} - \zeta \varepsilon^{-1} \frac{\partial \kappa}{\partial x} \right. \right. \\ &\quad \left. \left. + 2\zeta^2 \kappa^2 h_x + 4\zeta^2 \kappa h \frac{\partial \kappa}{\partial x} \right) \right] \\ &\quad + \zeta \kappa SS \left(\frac{1}{2} y^3 - \frac{3}{2} hy^2 + 3h^2 y \right). \end{aligned} \tag{47}$$

Now from the continuity equation we have

$$\partial_t h = -3SSh^2 h_x. \tag{48}$$

Putting this in (47) we get

$$\begin{aligned} u_1 &= \text{Re} SS^2 \left(\frac{3}{8} hy^4 - \frac{3}{2} h^2 y^3 + 3h^4 y \right) h_x \\ &\quad - \frac{9}{2} \text{Re} \Gamma SS^2 y h (y - 2h) h_x + \text{Re} \left(\frac{y^2}{2} - hy \right) \\ &\quad \times \left[\frac{3CS}{\text{Re}} h_x - \varepsilon^2 \text{We} \left(h_{xxx} - \zeta \varepsilon^{-1} \frac{\partial \kappa}{\partial x} + 2\zeta^2 \kappa^2 h_x \right. \right. \\ &\quad \left. \left. + 4\zeta^2 \kappa h \frac{\partial \kappa}{\partial x} \right) \right] + \zeta \kappa SS \left(\frac{1}{2} y^3 - \frac{3}{2} hy^2 + 3h^2 y \right), \end{aligned} \tag{49}$$

$$\begin{aligned} q_1 &= \int_0^h u_1 dy \\ &= \frac{6}{5} \text{Re} SS^2 h^6 h_x + 3 \text{Re} SS^2 \Gamma h^4 h_x \\ &\quad - \frac{1}{3} \text{Re} h^3 \left[\frac{3CS}{\text{Re}} h_x - \varepsilon^2 \text{We} \left(h_{xxx} - \zeta \varepsilon^{-1} \frac{\partial \kappa}{\partial x} \right. \right. \\ &\quad \left. \left. + 2\zeta^2 \kappa^2 h_x + 4\zeta^2 \kappa h \frac{\partial \kappa}{\partial x} \right) \right] + \frac{9}{8} \zeta \kappa SS h^4. \end{aligned} \tag{50}$$

Integrating the continuity equation, (21), with respect to y from 0 to h by using Leibniz's rule and boundary conditions

(24) and (27), we have

$$\frac{\partial h}{\partial t} + (1 - \varepsilon \zeta \kappa h) \left(\frac{\partial q_0}{\partial x} + \varepsilon \frac{\partial q_1}{\partial x} \right) + O(\varepsilon^2) = 0. \quad (51)$$

Substituting the values of q_0 and q_1 from (46) and (50) we get

$$h_t + A(h)h_x + \varepsilon(B(h)h_x + \varepsilon^2 C(h)h_{xxx})_x = 0, \quad (52)$$

where the suffix denotes the differentiation with respect to the corresponding variables and

$$A(h) = 3 \left(SS - Bo \zeta \frac{\partial \kappa}{\partial x} \right) h^2 + \varepsilon \zeta \kappa \left[\frac{3}{2} SS + 16Bo \zeta \frac{\partial \kappa}{\partial x} \right] h^3, \quad (53)$$

$$B(h) = \left[\frac{6}{5} ReSS^2 h^3 + 3ReSS^2 \Gamma h - CS + 2Bo \zeta^2 \kappa^2 \right] h^3, \quad (54)$$

$$C(h) = \frac{1}{3} WeReh^3, \quad (55)$$

where $Bo (\equiv 4\pi^2 s_0 / \rho g \lambda^2 \sin \beta)$ is the inverse Bond number and is connected by the relation $\varepsilon^2 ReWe = 3Bo$.

We would like to introduce a nondimensional parameter, $Fi (\equiv s_0^3 / \rho^3 g \sin \beta v^4)$, which is called the *film number* by Alekseenko *et al.* [2] for a vertical film. We revisit here the definition of the *Weber number* as $We (\equiv 3Fi/Re^5)^{1/3}$.

IV. LINEAR STABILITY ANALYSIS

Our interest in this section is to discuss the linear stability analysis from two important perspectives. First we discuss the instability localized in space, i.e., *spatial instability*. This kind of instability occurs in most natural flows, laboratory experiments, and technical and industrial applications, where the instability is triggered at a certain point in the space and advance spatially.

On the other hand, we discuss the temporal progression of disturbances, keeping the periodicity of the spatial flow fixed, i.e., *temporal instability*. This kind of study is important in analytical modeling of instability and study of weakly nonlinear analysis.

A. Spatial instability

Using the expression of u_1 from (47) and computing q_1 in the same way as before, we may substitute in (51) in order to get the first-order surface equation as

$$h_t + A(h)h_x + \varepsilon \left[ReSS \left(\frac{3}{2} \Gamma h^2 - \frac{5}{8} h^4 \right) h_t - ReSS^2 \left(-\frac{9}{2} \Gamma h^4 + \frac{15}{8} h^6 \right) h_x + B(h)h_x + \varepsilon^2 C(h)h_{xxx} \right]_x. \quad (56)$$

We now intend to use the normal-mode solution at $h = 1$. We may write

$$h(x, t) = 1 + \Lambda \exp [ik(x - ct)] + c.c., \quad (57)$$

where $c, k \in \mathbb{C}$ are the wave speed and wave number, respectively, $\Lambda \in \mathbb{C}$ is the amplitude of the disturbance ($\Lambda \ll 1$), and c.c. stands for complex conjugate.

After making the transformation $t \rightarrow \varepsilon t$ and $x \rightarrow \varepsilon x$, substituting (57) in the transformed form of (56), and using a Taylor-series expansion about $h = 1$, the linearized equation can be written as

$$i(c - c_k) + k ReSS \left(\frac{5}{8} - \frac{3}{2} \Gamma \right) (c - c_d) = 0, \quad (58)$$

where

$$c_k = A_1, \quad (59)$$

$$c_d = \frac{1}{ReSS \left(\frac{5}{8} - \frac{3}{2} \Gamma \right)} \left[-B_1 - ReSS^2 \left(\frac{9}{2} \Gamma - \frac{15}{8} \right) + C_1 k^2 \right], \quad (60)$$

where A_1, B_1 , and C_1 are, respectively, the values of A, B , and C evaluated at $h = 1$.

Equation (58) is a combination of two wave equations. Whitham [47] introduced this kind of wave structure first. One of them represents higher-order waves dispersive in nature, moving at speed c_d ; these are called *dynamic waves*. This kind of wave is not associated with the transport in the fluid, and its velocity is dependent on the fluid inertia, gravity, and surface tension. On the contrary, the other family of waves involved in (58) is *kinematic waves*. These are lower-order waves moving at a speed c_k and responsible for transport in the fluid. In our case the *kinematic wave* is nondispersive in nature and are expected to be a low-frequency distribution [48].

The localized initial perturbation originates a wave packet which supplies energy to the mean flow. The energy is then supplied to the kinematic wave through the higher-order wave mechanism from mean flow and this process is controlled with a small Reynolds number. Next this energy is transferred to the dynamic wave with a higher Reynolds number mechanism. The condition for the surface wave to be stable, neutral, or unstable comes from the intersection, i.e.,

$$c_k \leq c_d, \quad (61)$$

i.e.,

$$A_1 \leq \frac{1}{ReSS \left(\frac{5}{8} - \frac{3}{2} \Gamma \right)} \left[-B_1 + ReSS^2 \left(\frac{9}{2} \Gamma - \frac{15}{8} \right) + C_1 k^2 \right]. \quad (62)$$

Condition (61) is derived from the evolution of the wave packet. The tendency of the kinematic wave is to turn out from the wave packet at long times, whereas the dynamic wave dominates the mechanism with a short-term gesture. So, the only possibility for stability is when the dynamic wave makes the back and the front of the wave packet. In practice, when $c_k = c_d$ instability arises.

We have used the continuation software AUTO07p [49] to numerically solve the dispersion relation, (58), and the results are presented as a case study in Sec. IX.

B. Temporal instability

Here we follow the standard linear stability analysis for the temporal case [48,50,51]. We give an initial sinusoidal perturbation of the form $h(x, t) = 1 + \Lambda \exp [i(kx - \omega t)] + c.c.$, where $\Lambda \in \mathbb{C}$ is the amplitude of the disturbance and c.c. stands for the complex conjugate. The wave number $k \in \mathbb{R}$

and the frequency $\omega \in \mathbb{C}$. After making the transformation $t \rightarrow \varepsilon t$ and $x \rightarrow \varepsilon x$ the linearized part of the transformed form of Eq. (52) can be written in the form

$$\text{Disp}(\omega, k) \equiv i(\omega - A_1 k) + B_1 k^2 - C_1 k^4 = 0. \quad (63)$$

Equating the real and the imaginary parts of (63) we get

$$\omega_r = A_1 k \quad \text{and} \quad \omega_i = B_1 k^2 - C_1 k^4. \quad (64)$$

So, the linear phase velocity is

$$c_r = \frac{\omega_r}{k} = A_1. \quad (65)$$

In this case it appears that the linear phase velocity in the temporal case is equal to the kinematic wave speed in the spatial case. Again, the wave is nondispersive in nature, as the linear phase velocity is also independent of k . The imaginary part of c is given by

$$c_i = \frac{\omega_i}{k} = B_1 k - C_1 k^3. \quad (66)$$

The flow will be linearly stable if $\omega_i < 0$ (or $c_i < 0$). From here we get the critical Reynolds number as

$$\text{Re}_c = \frac{CS - 2\text{Bo}\zeta^2\kappa^2}{\frac{3}{5}SS^2(2 + 5\Gamma)}. \quad (67)$$

For Newtonian fluid flow over a wavy bottom $\Gamma \rightarrow 0$ we get the result found by Mukhopadhyay and Mukhopadhyay [48]:

$$\text{Re}_c = \frac{CS - 2\text{Bo}\zeta^2\kappa^2}{\frac{6}{5}SS^2}. \quad (68)$$

It is to be noted here that when $\zeta \rightarrow 0$, $\theta \rightarrow 0$, i.e., for viscoelastic film flowing over a flat surface we retrieve

$$\text{Re}_c = \frac{5}{6} \cot \beta (1 + \frac{5}{2}\Gamma)^{-1},$$

which is the same as the result derived by Mukhopadhyay and Haldar [52] if we consider $Mn \rightarrow 0$ as in their paper.

Again, as $\zeta \rightarrow 0$, $\theta \rightarrow 0$, and $\Gamma \rightarrow 0$, i.e., for a Newtonian film over a flat surface, $\text{Re}_c = \frac{5}{6} \cot \beta$, which is the established result of Benjamin [8] and Yih [9]. The cutoff wave number can be found as

$$k_c = \left(\frac{B_1}{C_1} \right)^{1/2}. \quad (69)$$

Now for a moderately small steepness, we can write

$$\kappa = \kappa_0 + \zeta^2 \kappa_2 + O(\zeta^4), \quad \theta = \zeta \theta_1 + O(\zeta^3), \quad (70)$$

where $\theta_1 = \partial \hat{b}(x) / \partial \hat{x}$, $\kappa_0 = -\partial^2 \hat{b}(x) / \partial \hat{x}^2$, and

$$\begin{aligned} \frac{\cos(\beta - \theta)}{\sin \beta} &= \cot \beta + \zeta \theta_1 - \frac{1}{2} \zeta^2 \theta_1^2 \cot \beta + O(\zeta^3), \\ \frac{\sin(\beta - \theta)}{\sin \beta} &= 1 - \zeta \theta_1 \cot \beta - \frac{1}{2} \zeta^2 \theta_1^2 + O(\zeta^3). \end{aligned} \quad (71)$$

For details about the above expansion we refer the reader to Hacker *et al.* [39] Then relation (68) approximates to

$$\begin{aligned} \text{Re}_c &= \frac{5}{6} [\cot \beta + \zeta(1 + 2\cot^2 \beta)\theta_1 \\ &\quad + \zeta^2((\frac{5}{2} + 3\cot^2 \beta)\cot \beta \theta_1^2 - \text{Bo}\kappa_0^2)]. \end{aligned} \quad (72)$$

Relation (72) is in fairly very good agreement with Eq. (61) of Wierschem *et al.* [28] [with our scaling and assumptions up to $O(\zeta^2)$].

The term $\zeta^2 \kappa^2 \text{Bo}$ in Eq. (67) is of order ε^2 and has a negligible impact. This term can be neglected, but we retain the term in our expression, only to compare the result with Wierschem *et al.* [28].

V. WEAKLY NONLINEAR ANALYSIS

We need the weakly nonlinear analysis for a small but finite amplitude of disturbance, because the linear theory can no longer predict the behavior of the flow correctly. The role of the weakly nonlinear analysis is to investigate whether a finite amplitude disturbance can cause instability in the linearly stable region (subcritical instability), or the nonlinear evolution of a finite amplitude disturbance can develop a new equilibrium state in a linearly unstable region (supercritical instability), or the disturbance grows towards instability.

Before proceeding to the main discussion we would like to elaborate on the discussion about normal-mode analysis. Equation (52) has a normal-mode solution of the form $h(x, t) = 1 + \eta(x, t)$ for a parallel shear flow, where $\eta(x, t) \in \mathbb{C}$ is the disturbance and $\eta(x, t) \ll 1$. After taking the transformation $t \rightarrow \varepsilon t$ and $x \rightarrow \varepsilon x$ using a Taylor-series expansion about $h = 1$, Eq. (52) can be written as

$$\begin{aligned} \eta_t + A_1 \eta_x + B_1 \eta_{xx} + C_1 \eta_{xxx} + \left[A_1' \eta + \frac{A_1''}{2} \eta^2 \right] \eta_x \\ + \left[B_1' \eta + \frac{B_1''}{2} \eta^2 \right] \eta_{xx} + \left[C_1' \eta + \frac{C_1''}{2} \eta^2 \right] \eta_{xxx} \\ + (B_1' + B_1'' \eta) \eta_x^2 + (C_1' + C_1'' \eta) \eta_x \eta_{xxx} + O(\eta^4) = 0, \end{aligned} \quad (73)$$

where A_1 , B_1 , and C_1 and their corresponding derivatives with respect to h , which are denoted by primes, are evaluated at $h = 1$.

We now use the method of multiple scale [53] to derive the complex Ginzburg-Landau-type equation from (73). In the vicinity of criticality, the slow independent variables are defined as

$$X = \alpha x, \quad T_1 = \alpha t, \quad T_2 = \alpha^2 t, \quad (74)$$

where α is the weakness of the nonlinearity. Now

$$\frac{\partial}{\partial t} \rightarrow \frac{\partial}{\partial t} + \alpha \frac{\partial}{\partial T_1} + \alpha^2 \frac{\partial}{\partial T_2}, \quad (75)$$

$$\frac{\partial}{\partial x} \rightarrow \frac{\partial}{\partial x} + \alpha \frac{\partial}{\partial X}. \quad (76)$$

The solution of (73) is expanded in power series of α as

$$\eta(x, X, t, T_1, T_2) = \sum_{i=1}^{\infty} \alpha^i \eta_i(x, X, t, T_1, T_2). \quad (77)$$

Substituting (74) and (77) in (52) we get

$$\begin{aligned} (L_0 + \alpha L_1 + \alpha^2 L_2)(\alpha \eta_1 + \alpha^2 \eta_2 + \alpha^3 \eta_3) \\ = -\alpha^2 N_2 - \alpha^3 N_3 - \dots, \end{aligned} \quad (78)$$

where L_0, L_1 , and L_2 are the operators given by

$$\begin{aligned} L_0 &= \frac{\partial}{\partial t} + A_1 \frac{\partial}{\partial x} + B_1 \frac{\partial^2}{\partial x^2} + C_1 \frac{\partial^4}{\partial x^4}, \\ L_1 &= \frac{\partial}{\partial T_1} + A_1 \frac{\partial}{\partial X} + 2B_1 \frac{\partial^2}{\partial x \partial X} + 4C_1 \frac{\partial^4}{\partial x^3 \partial X}, \quad (79) \\ L_2 &= \frac{\partial}{\partial T_2} + B_1 \frac{\partial^2}{\partial X^2} + 6C_1 \frac{\partial^4}{\partial x^2 \partial X^2}, \end{aligned}$$

and N_2 and N_3 are the nonlinear terms given by

$$\begin{aligned} N_2 &= A'_1 \eta_1 \eta_{1x} + B'_1 \eta_1 \eta_{1xx} + C'_1 \eta_1 \eta_{1xxx} \\ &\quad + B'_1 \eta_{1x}^2 + C'_1 \eta_{1x} \eta_{1xxx}, \quad (80) \end{aligned}$$

$$\begin{aligned} N_3 &= A'_1 (\eta_1 \eta_{2x} + \eta_1 \eta_{1X} + \eta_2 \eta_{1x}) + \frac{A''_1}{2} \eta_1^2 \eta_{1x} \\ &\quad + B'_1 (\eta_1 \eta_{2xx} + 2\eta_1 \eta_{1xX} + \eta_2 \eta_{1xx}) \\ &\quad + C'_1 (\eta_1 \eta_{2xxx} + 4\eta_1 \eta_{1xxxX} + \eta_2 \eta_{1xxx}) \\ &\quad \times B'_1 (2\eta_{1x} \eta_{2x} + 2\eta_{1x} \eta_{1X}) \\ &\quad + C'_1 (\eta_{2xxx} \eta_{1x} + 3\eta_{1xxX} \eta_{1x} + \eta_{1xxx} \eta_{2x} + \eta_{1xxx} \eta_{1X}) \\ &\quad + \frac{B''_1}{2} \eta_1^2 \eta_{1xx} + \frac{C''_1}{2} \eta_1^2 \eta_{1xxx} B_1 c_3'' \eta_1 \eta_{1x}^2 \\ &\quad + C''_1 \eta_1 \eta_{1x} \eta_{1xxx}. \quad (81) \end{aligned}$$

The disturbance $\eta(x, t)$ is decomposed as $\eta(x, t) = \Lambda \exp[i(kx - \omega t)] + \text{c.c.}$, where $\Lambda \in \mathbb{C}$ is the amplitude of the disturbance and c.c. stands for complex conjugate. We solved the equations order by order using the solvability condition up to $O(\alpha^3)$. We obtain an equation related to the complex Ginzburg-Landau equation of the perturbation amplitude,

$$\frac{\partial \Lambda}{\partial T_2} + iV \frac{\partial \Lambda}{\partial X} + J_1 \frac{\partial^2 \Lambda}{\partial X^2} - \omega'_i \Lambda + (J_2 + iJ_4) |\Lambda|^2 \Lambda = 0, \quad (82)$$

where

$$\begin{aligned} \omega'_i &= \alpha^{-2} \omega_i, \\ V &= 2k(B_1 - 2C_1 k^2) \alpha^{-1}, \\ J_1 &= B_1 - 6C_1 k^2, \quad (83) \\ J_2 &= 7k^4 e_r C'_1 - k^2 e_r B'_1 - \frac{k^2}{2} B''_1 + \frac{k^4}{2} C''_1 - k e_i A'_1, \\ J_4 &= 7k^4 e_i C'_1 - k^2 e_i B'_1 + k e_r A'_1 + k \frac{A''_1}{2}, \end{aligned}$$

where

$$e_r = \frac{2(B'_1 - k^2 C'_1)}{(-4B_1 + 16k^2 C_1)}, \quad e_i = \frac{-A'_1}{k(-4B_1 + 16k^2 C_1)}.$$

We now investigate the weakly nonlinear behavior of the flow from Eq. (82). The assumption to solve (82) has been taken as the wave is filtered, i.e., there is no spatial modulation so the diffusion term vanishes.

For a filtered wave the solution of Eq. (82) may be written as

$$\Lambda = \Lambda_0(T_2) \exp[-i b(T_2) T_2]. \quad (84)$$

Substituting the above relation in Eq. (82) we get

$$\frac{\partial \Lambda_0}{\partial T_2} = (\alpha^{-2} \omega_i - J_2 \Lambda_0^2) \Lambda_0 \quad (85)$$

and

$$\frac{\partial (b(T_2) T_2)}{\partial T_2} = J_4 \Lambda_0^2. \quad (86)$$

Due to the nonlinearity, the term $(J_2 \Lambda_0^2) \Lambda_0$ appears on the right-hand side of Eq. (85). This term may accelerate or decelerate the exponential growth of the linear disturbance.

The threshold amplitude is given by

$$\alpha \Lambda_0 = \left[\frac{\omega_i}{J_2} \right]^{\frac{1}{2}}. \quad (87)$$

The nonlinear wave speed will be

$$Nc_r = c_r + c_i \frac{J_4}{J_2}. \quad (88)$$

Here the nonlinear wave speed given in (88) is dispersive in nature, contrary to the linear wave speed discussed earlier.

Here J_2 plays an important role in the study of weakly nonlinear analysis, because if $J_2 = 0$, Eq. (85) becomes a linear partial differential equation of the filtered waves and the amplitude grows and decays exponentially when $\omega_i < 0$ or $\omega_i > 0$. When $J_2 \neq 0$ the nonlinear stability depends on the sign of J_2 . The bifurcation is supercritical when $J_2 > 0$ and subcritical when $J_2 < 0$, i.e., anyway J_2 predicts the ultimate behavior of the system.

VI. TRAVELING WAVE SOLUTION

We are now interested in *traveling waves*. These periodic waves are computed as a stationary solution in a moving reference frame $\chi = x - ct$, where c is the speed of the wave as well as the speed of the frame. First using the transformation $t \rightarrow \varepsilon t$ and $x \rightarrow \varepsilon x$, then making the transformation $\chi = x - ct$ in (52), we get a fourth-order ordinary differential equation (ODE). Integrating once, finally, we achieve a third-order ODE as

$$-ch + P(h) + B(h)h' + C(h)h''' - q_0 = 0, \quad (89)$$

where $P(h) = \int A(h)h' d\chi$, primes denote the derivatives with respect to χ , and q_0 is the integration constant, which corresponds to the rate of flow of the fluid under the wave in the moving frame. As the wave moves faster than the flow, q_0 is negative.

The differential equation, (89), is solved iteratively with the continuation software AUTO07p by recasting it into a three-dimensional dynamical system. The continuation starts from the *Hopf bifurcation* point, and we have taken the sinusoidal initial perturbation of the form $1 - \bar{A} \sin(2f\pi x/l)$, where \bar{A} is the amplitude of the linear perturbation, f is the harmonic parameter, and $l = 2\pi/k$ is the period of the wave. We have mapped the domain to a domain of length unity via the transformation $x \rightarrow x/L$ for our convenience.

VII. NUMERICAL SIMULATIONS

We are interested in solving (52) numerically in a periodic domain to understand the evolution of finite-amplitude perturbation. This mechanism is responsible for the energy transfer from the basic state to the disturbance. We use Scikit-FDif [54], a tool written in PYTHON which uses the finite-difference method to discretize the spatial derivative and the method of lines to transform the original partial differential equation into a high-dimension ODE that can be solved simply by standard numerical integration of the ODE. These provide fast computation of the Jacobian matrix and the temporal evolution vector.

Initially, we impose a finite-amplitude monochromatic disturbance as

$$h(x, 0) = 1 + 0.1 \cos(2\pi x/L). \quad (90)$$

As we know from Joo *et al.* [55], the finite state of disturbance is insensitive to the amplitude of the primary disturbance. $L = 2\pi/k$ is the length of the periodic domain and k is the wave number. We examine the structure of the wave in the variable length domain L as the wave number k varies so it is more convenient to map this domain to a domain of length unity via $x \rightarrow x/L$. The computation is performed on a uniform grid, with the number of spatial grid points varying between $N = 600$ and $N = 800$ ($\Delta x = 1/N \sim 1.2 \times 10^{-3} - 1.6 \times 10^{-3}$) and between $\Delta t = 0.05 - 0.5$ and $\Delta t = 0.5$. We discuss the authenticity of the results of our case studies in detail in Sec. IX.

VIII. CASE STUDY

So far to discuss the problem we have used a general wavy bottom profile \hat{b} . The specific form of the bottom topography does not enter into the problem yet; the approach as discussed so far is applicable to other periodic contours as well.

Now for a case study we choose a sinusoidal bottom profile,

$$\hat{b}(\hat{x}) = \hat{a} \cos(2\pi \hat{x}/\hat{\lambda}), \quad (91)$$

where $\hat{\lambda}$ is the wavelength and \hat{a} is the amplitude of the wavy bottom profile. Furthermore, for the numerical investigation afterward we take $\hat{\lambda} = 300$ mm, $\hat{a} = 15$ mm, and the downhill portion is $0.0 \text{ mm} < \hat{a} < 150$ mm whereas the uphill portion is $150 \text{ mm} < \hat{a} < 300$ mm. $\hat{x} = 0.0$ mm is the crest and $\hat{x} = 150$ mm is the ‘‘trough.’’ We refer to Fig. 1 for better understanding. Finally, we would like to mention here that the bottom steepness is taken as moderately small, yet it enters as a fixed quantity and not as a perturbation parameter. Since both the bottom curvature $\kappa(\hat{x})$ and the local inclination $\theta(\hat{x})$ are functions of \hat{x} , Re_c will also be a function of \hat{x} that is $\text{Re}_c(\hat{x})$.

To specify the properties of the viscoelastic fluid we have chosen fluids having three different viscoelastic parameter Γ values ($\Gamma = 0.06, 0.2$, and 0.4) depending upon the properties of the fluids. One of them is the mixture of polymethyl methacrylate and pyridine at 25°C , containing 30.5 g of polymer per liter, which behaves very close to our model. The physical properties with such a fluid constitute its density $\rho = 0.98 \times 10^{-3} \text{ kg/m}^3$, limiting viscosity $\mu = 0.79 \text{ N s/m}^2$, sur-

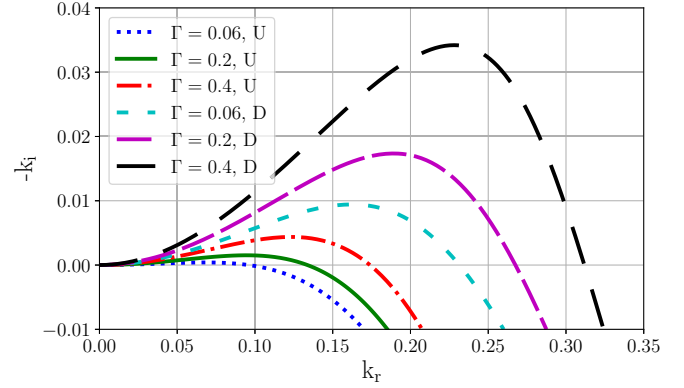


FIG. 2. Spatial growth rate curve for different viscoelastic parameters at a point in the uphill (U; $x = 4.71$) and at a point in the downhill (D; $x = 1.57$) region for $\zeta = 0.1\pi$, $\text{Re} = 1.5$.

face tension $s_0 = 40 \times 10^{-3} \text{ N/m}$, and viscoelastic coefficient $\gamma_0 = 0.04 \text{ N s}^2/\text{m}^2$. Unless stated otherwise, the film number is taken as $\text{Fi} = 3.7 \times 10^{11}$ and $\varepsilon = 0.01$.

IX. RESULTS AND DISCUSSION

We now discuss the results part by part taking the reference stated in Sec. VIII. Our main focus in this study is to analyze the effect of bottom topography as well as the non-Newtonian property of a viscoelastic fluid in the hydrodynamics of flow. We have formulated the problem by transforming the governing equations and the associated boundary conditions in the curvilinear coordinate system. This kind of transformation is important for discussing easily the problems containing a curvy topography. Our basic assumption for the entire study is that the film is thin, the bottom profile is periodic, and the bottom steepness is moderate. But notwithstanding this, the dependence of the surface on the local inclination angle ($\beta - \theta$) strongly restricts the maximum steepness for a given inclination angle β [28]. After critical numerical observations we have chosen the range of the bottom steepness ζ from 0.0 to 0.4 for the inclination angle $\beta = \pi/3$ to make the model physically and geometrically consistent. A surface evolution equation is then derived using the classical long-

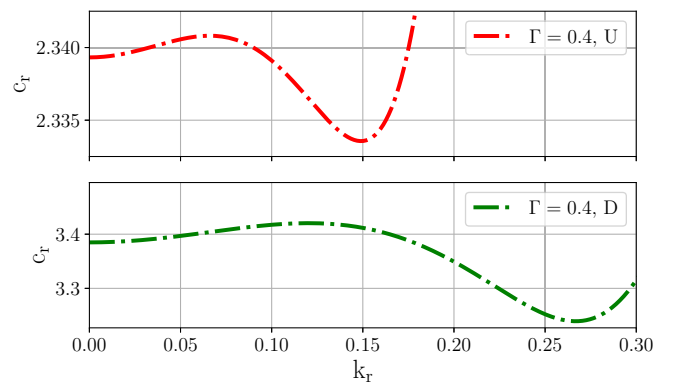


FIG. 3. Phase speed along the growth rate curve at a point in the uphill (U; $x = 4.71$) and at a point in the downhill (D; $x = 1.57$) region for $\Gamma = 0.4$, $\zeta = 0.1\pi$, $\text{Re} = 1.5$.

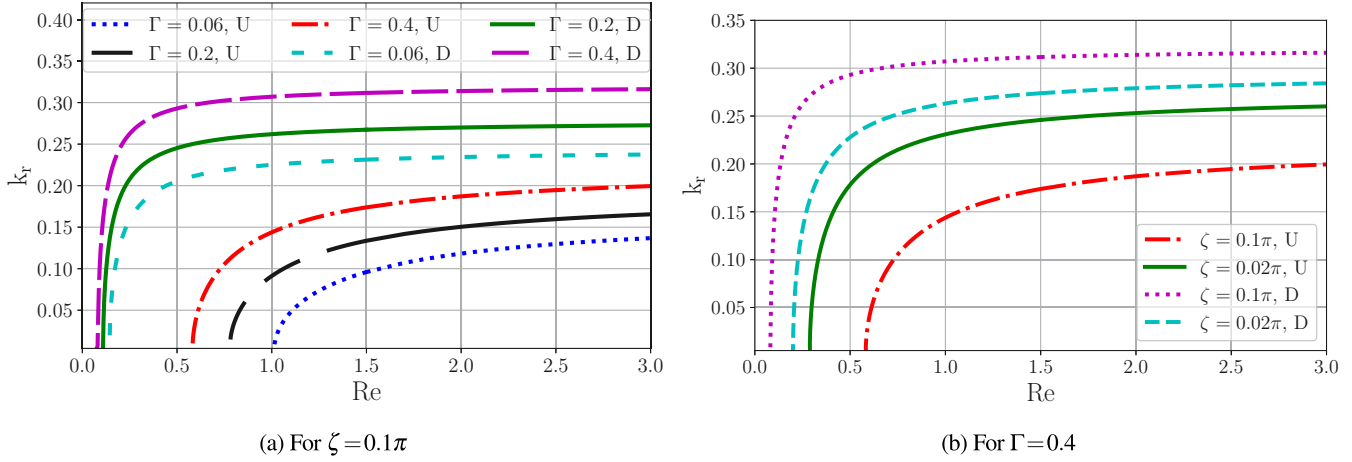


FIG. 4. Marginal stability curve (a) for different viscoelastic parameters keeping ζ the same and (b) for different bottom steepnesses keeping Γ the same, at a point in the uphill (U; $x = 4.71$) and at a point in the downhill (D; $x = 1.57$) region.

wave expansion method accounting for the basic physical properties of the fluid, the topographic nature of the bottom, and other important characteristics such as gravity and mean surface tension in terms of different nondimensional numbers.

A. Results of the linear stability analysis

In this section, we discuss the results of the linear stability analysis in two subsections. First, we discuss the spatial case and then the temporal case.

1. Spatial case

From the discussion in Sec. IV A, we analyze some important results in this section for the sinusoidal bottom topography, (91). Figure 2 represents the spatial growth rate $-k_i$ versus the wave number k_r for $Re = 1.5$ for different viscoelastic parameters Γ at a point in the uphill and at a point in the downhill region for a moderate bottom steepness ($\zeta = 0.1\pi$). The spatial growth rate $-k_i$ determines how the

system will react to a harmonic perturbation with a real angular frequency ω at the inlet. $-k_i > 0$ indicates that the perturbation is amplified downstream with a contrary of $-k_i < 0$, which indicates that the perturbation is damped and hence the system is stable. As we can see, in both the downhill and the uphill regions an increasing Γ increases $-k_i$ in the positive direction, i.e., the greater value of the viscoelastic parameter Γ , the more unstable the flow. But one interesting thing is that the uphill region gives a comparatively more stable effect than the downhill region for a fixed Γ . The reason for this is supported by Fig. 3, where we have compared the phase speed of the wave along the growth rate curve at a point in the uphill and at a point in the downhill region for a fixed $\Gamma = 0.4$ and $Re = 1.5$. The phase speed c_k is more for the downhill region. Figure 4(a) shows the marginal stability curve in the $Re-k$ plane for different Γ values at a point in the uphill and at a point in the downhill region. Again, the critical Reynolds number increases with decreasing Γ for both the uphill and the downhill regions, but the variation of the critical Re with Γ is more prominent in the uphill region than the downhill

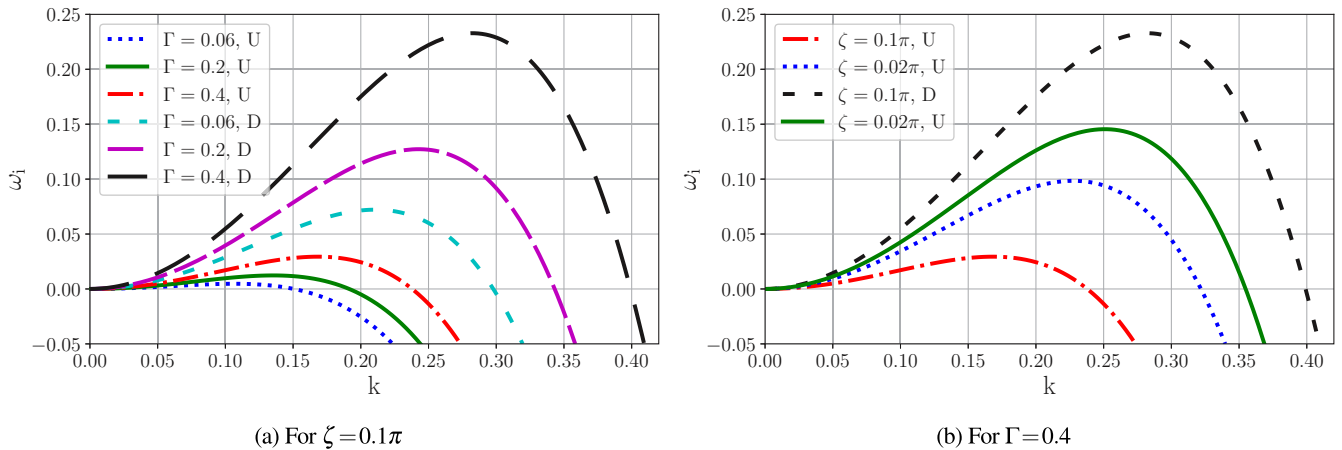


FIG. 5. Temporal growth rate curve (a) for different viscoelastic parameters keeping ζ the same and (b) for different bottom steepnesses keeping Γ the same, at a point in the uphill (U; $x = 4.71$) and at a point in the downhill (D; $x = 1.57$) region for $Re = 2$. (a) Supercritical, $Re = 1 : 3$, $Bo = 0 : 04$ and (b) Subcritical, $Re = 5$, $Bo = 0 : 04$.

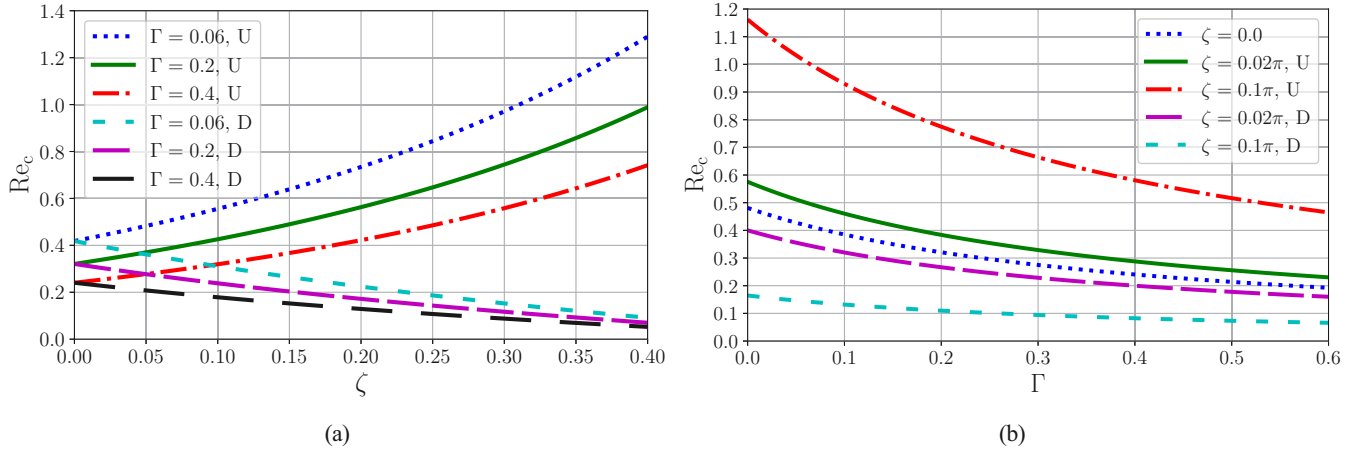


FIG. 6. Critical Reynolds number (a) as a function of the bottom steepness for different Γ values and (b) as a function of the viscoelastic parameter for different ζ values, at a point in the uphill (U; $x = 4.71$) and at a point in the downhill (D; $x = 1.57$) region.

portion. We can conclude for the linear stability analysis that the effect of the bottom topography is more prominent than the effect of the viscoelasticity of the fluid. Figure 4(b) shows the variation of marginal stability with the bottom steepness ζ for a fixed Γ at a point in the uphill and at a point in the downhill region. A dual effect of ζ is found here. In the uphill region, an increasing ζ gives stability and the opposite occurs for the downhill region. This is a very interesting phenomenon, and we explain it in detail later.

2. Temporal case

Figure 5(a) shows the temporal growth rate for different Γ values at a point in the uphill and at a point in the downhill region for $Re = 2$, and Fig. 5(b) shows the same but for a fixed Γ with a variation of the bottom steepness ζ . In the case of the temporal stability analysis we see the same trend of results as seen in the spatial case. Increasing Γ destabilizes the system and ζ plays a dual role for the uphill and downhill regions. In support of this argument we have plotted the

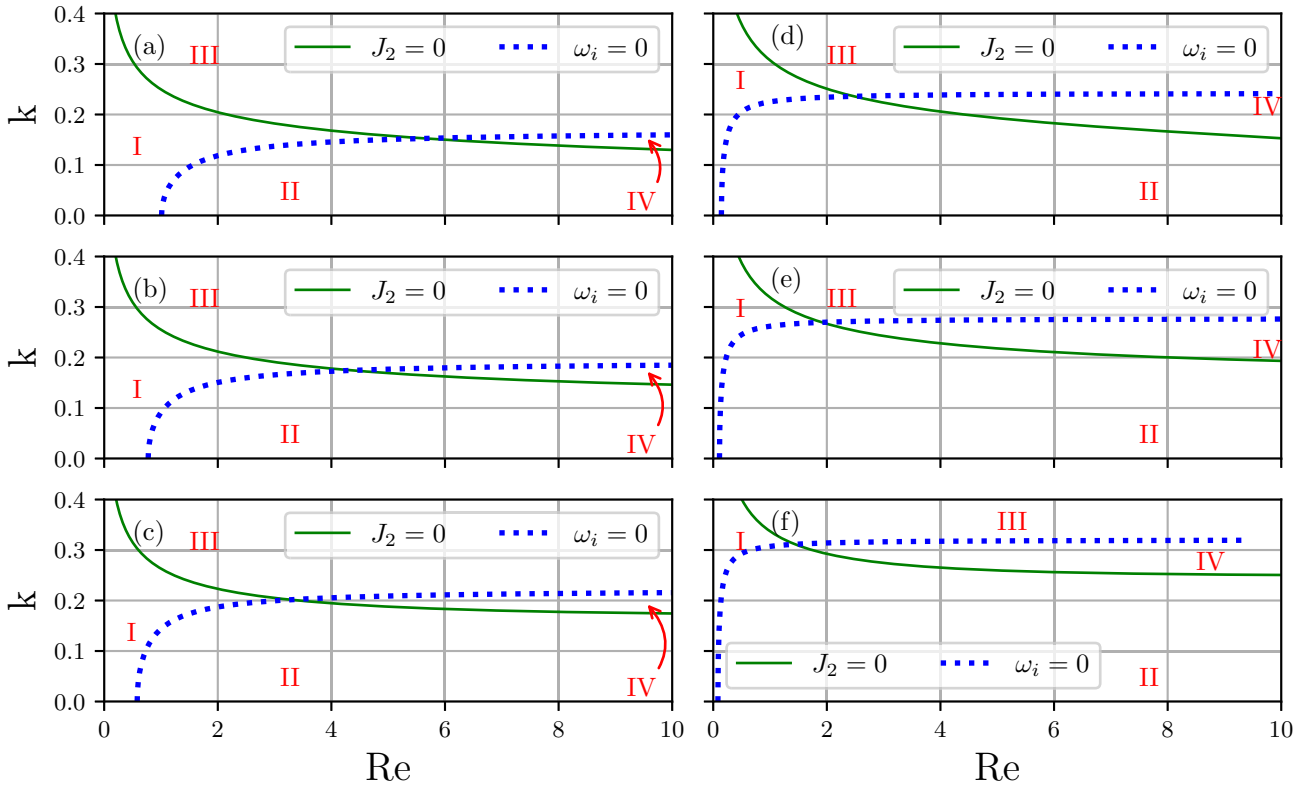


FIG. 7. Stability curve at a point in the uphill (U; $x = 4.71$) and at a point in the downhill (D; $x = 1.57$) region for different Γ values. Regions indicated in the plot: I, unconditional; II, supercritical; III, subcritical; and IV, explosive. (a) $\Gamma = 0.06, U$; (b) $\Gamma = 0.2, U$; (c) $\Gamma = 0.4, U$; (d) $\Gamma = 0.06, D$; (e) $\Gamma = 0.2, D$; (f) $\Gamma = 0.4, D$.

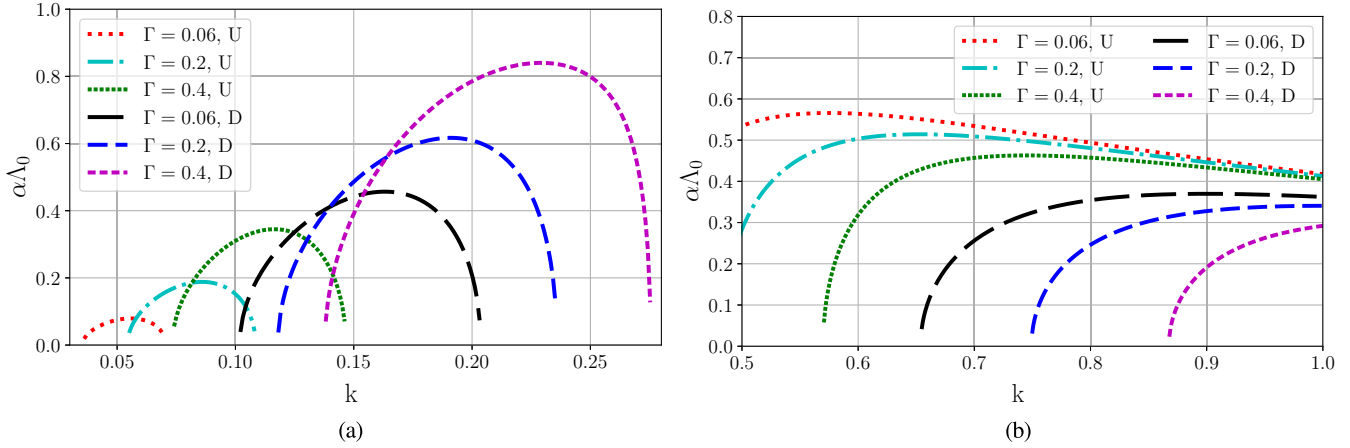


FIG. 8. Threshold amplitude of disturbances in the supercritical and subcritical regions at a point in the uphill (U; $x = 4.71$) and at a point in the downhill (D; $x = 1.57$) region for different Γ values. (a) Supercritical, $Re = 1.3$, $Bo = 0.04$ and (b) Subcritical, $Re = 5$, $Bo = 0.04$.

critical Reynolds number Re_c as a function of ζ keeping Γ to some fixed values in Fig. 6(a) and Re_c as a function of Γ keeping ζ to some fixed values in Fig. 6(b). Both in the uphill and in the downhill regions increasing Γ decreases the Re_c .

When $\zeta = 0$ and $\Gamma \rightarrow 0$ in Fig. 6(b) we retrieve the result for a Newtonian film flowing over a flat plate, and in that case we found the same results as Benjamin [8] and Yih [9], i.e., $Re_c = (5/6) \cot \beta \sim 0.48$ (as $\beta = \pi/3$).

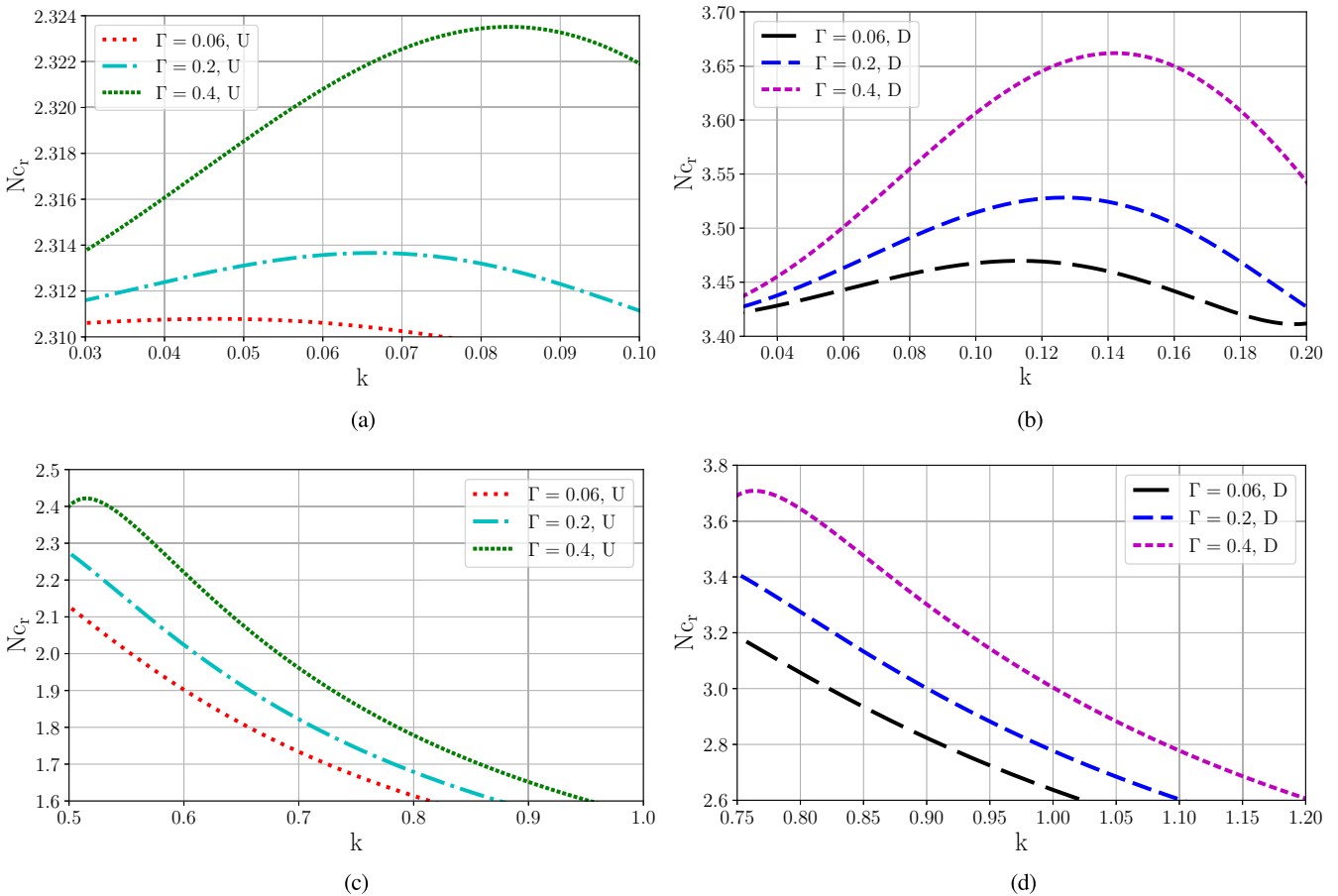


FIG. 9. Nonlinear wave speed in the supercritical and subcritical regions at a point in the uphill (U; $x = 4.71$) and at a point in the downhill (D; $x = 1.57$) region for different Γ values. (a) Supercritical Uphill, $Re = 1.3$, $Bo = 0.04$, (b) Supercritical Downhill, $Re = 1.3$, $Bo = 0.04$, (c) Subcritical Uphill, $Re = 5$, $Bo = 0.04$, and (d) Subcritical Downhill, $Re = 5$, $Bo = 0.04$.

B. Results of the weakly nonlinear analysis

We start with Fig. 7, which shows a stability diagram in the $Re-k$ plane for different Γ values at a point in the uphill and at a point in the downhill region. Different zones indicated in the graphs by I, II, III, and IV represent the following.

(1) *Zone I: Unconditional stable region.* Here $\omega_i < 0$ and $J_2 > 0$. In this region, finite-amplitude disturbances are unconditionally stable.

(2) *Zone II: Supercritical stable region.* Here $\omega_i > 0$ and $J_2 > 0$. In this linear unstable region, subsequent nonlinear growth of the disturbance will configure a new equilibrium state with a finite amplitude.

(3) *Zone III: Subcritical unstable region.* Here $\omega_i < 0$ and $J_2 < 0$. In the linear stable region, a finite-amplitude disturbance can create instability.

(4) *Zone IV: Explosive region.* Here $\omega_i > 0$ and $J_2 < 0$. In this region, instability increases and makes the system unstable.

In this problem with our case study, we found all four zones properly. We can see that fixing a Γ value, the unconditional stable zone increases and the explosive zone decreases in the uphill region more than in the downhill region. Once again it is proved that considering even the weak nonlinearity the uphill portion has a stabilizing effect for a particular bottom steepness. Another important result is shown in Fig. 7; with a fixed bottom region (uphill/downhill) increasing Γ increases the supercritical stable region. This phenomenon is more prominent for the downhill region than the uphill, i.e., the bottom topography has more impact on the flow than the viscoelastic property of the fluid. Figure 8(a) shows the threshold amplitude in the supercritical region, while Fig. 8(b) is the same for the subcritical region with Γ varied at a point in the uphill and at a point in the downhill region. In the supercritical stable region increasing Γ increases the amplitude of the nonlinear waves. The amplitude is more in the downhill portion than the uphill, while in the subcritical unstable region the opposite occurs. In this region, the nonlinear amplification rate is positive, while the linear amplification rate is negative, i.e., even if the linear theory predicts stability in this region, but actually if the disturbance is larger than the threshold amplitude, then the amplitude will

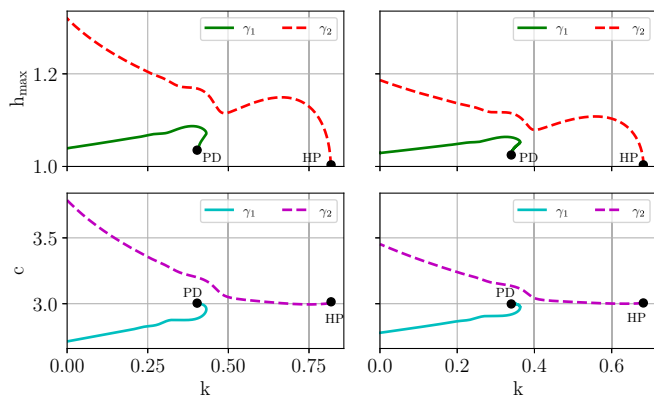


FIG. 10. Bifurcation diagram for different Γ and Re for $\zeta = 0.1\pi$. PD, period doubling; HP, Hopf bifurcation. Left column: $\Gamma = 0.4$, $Re = 12$. Right column: $\Gamma = 0.06$, $Re = 15$.

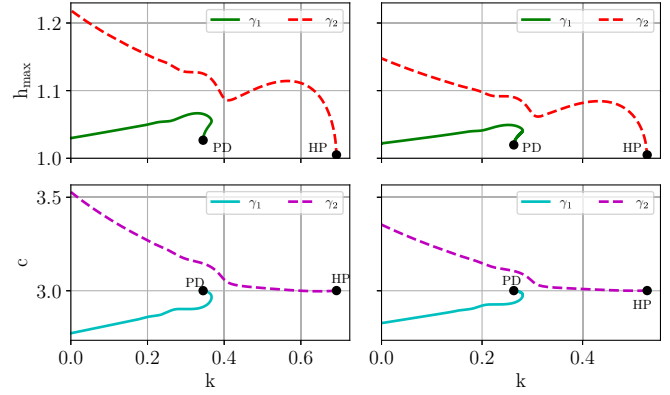


FIG. 11. Bifurcation diagram for different Γ and Re for $\zeta = 0.02\pi$. PD, period doubling; HP, Hopf bifurcation. Left column: $\Gamma = 0.4$, $Re = 15$. Right column: $\Gamma = 0.06$, $Re = 25$.

increase. Figure 9 shows the nonlinear wave speed Nc_r as a function of the wave number k for different Γ values at a point in the uphill and at a point in the downhill region for the supercritical stable and subcritical unstable regions. Both in the supercritical and in the subcritical region increasing Γ increases the nonlinear wave speed, which agrees with the result found by Mukhopadhyay and Halder [52] in the limiting case of the flat bottom. Also, in the downhill region the nonlinear speed is higher than in the uphill region, which agrees with the results of Mukhopadhyay and Mukhopadhyay [48] in the limiting case of a Newtonian fluid over a wavy bottom.

C. Results of the traveling wave solution

For this section we have used the periodic boundary condition for closed flow, i.e., the liquid which is flowing out of the domain is injected at the inlet periodically. Figures 10 and 11 represent bifurcation diagrams for different bottom steepnesses ζ and viscoelastic parameters Γ at different Reynolds numbers in terms of the maximum wave thickness h_{max} and phase speed c as a function of the wave number k . We

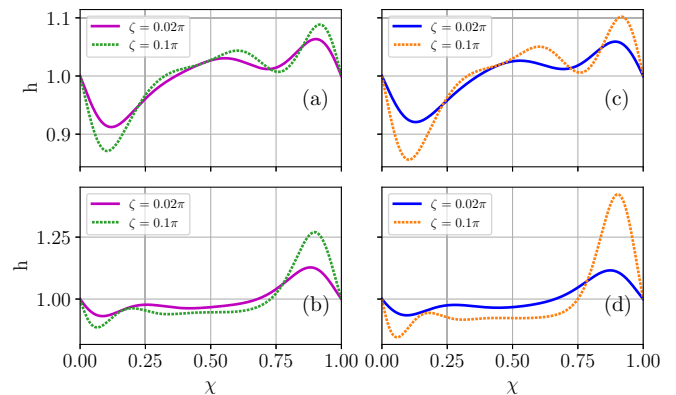


FIG. 12. Periodic stationary solutions of the γ_1 and γ_2 families for different Γ , Re , k and ζ . (a) $\Gamma = 0.4$, $k = 0.3$, $Re = 15$, γ_1 family; (b) $\Gamma = 0.4$, $k = 0.3$, $Re = 15$, γ_2 family; (c) $\Gamma = 0.06$, $k = 0.25$, $Re = 30$, γ_1 family; (d) $\Gamma = 0.06$, $k = 0.25$, $Re = 30$, γ_2 family.

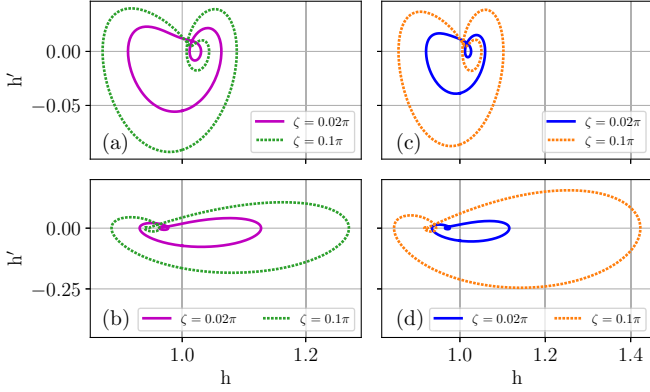


FIG. 13. Phase plane portraits for the traveling wave solution in Fig. 12. (a) $\Gamma = 0.4, k = 0.3, \text{Re} = 15, \gamma_1$ family; (b) $\Gamma = 0.4, k = 0.3, \text{Re} = 15, \gamma_2$ family; (c) $\Gamma = 0.06, k = 0.25, \text{Re} = 30, \gamma_1$ family; (d) $\Gamma = 0.06, k = 0.25, \text{Re} = 30, \gamma_2$ family.

have found that for viscoelastic flow down an inclined wavy bottom, starting from the critical wave number k_c as given in (69), if we gradually decrease k , different branches of traveling wave solutions ($\gamma_{1,2}$) bifurcate supercritically from neutral stability conditions through a Hopf bifurcation. The existence of two families, γ_1 and γ_2 , results from an *imperfect pitchfork bifurcation* [56], as identified earlier by Chang *et al.* [57] for a Newtonian fluid film flowing down a flat bottom. The existence of the γ_2 family can be seen for relatively small Reynolds numbers but in our case we found the γ_1 family for a moderate Re. It also is dependent on the values of Γ and ζ . This can be explained by the fact that the γ_1 waves normally have a lower traveling speed than the linear marginal waves. Again, the speed depends on the bottom topography as well. The uphill portion of the wall slows down the travel speed of the waves more than a flat film so to compensate for this fact we need a competitively high Re value in order to maintain the flow of the γ_1 family. A similar argument is found: as we decrease the bottom steepness ζ we need to increase Re slightly more in order to capture the characteristics of both the γ_1 and the γ_2 families. The γ_2 wave family consists of faster-moving waves starts from the Hopf bifurcation point.

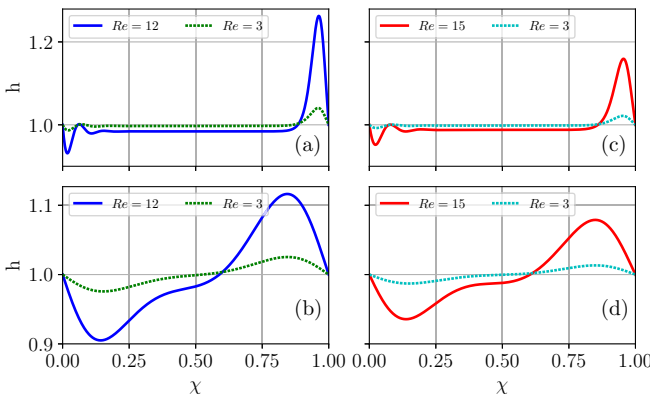


FIG. 14. Periodic stationary solutions of the γ_2 family for different Γ, Re , and k for $\zeta = 0.1\pi$. (a) $\Gamma = 0.4, k = 0.1$; (b) $\Gamma = 0.4, k = 0.5$; (c) $\Gamma = 0.06, k = 0.1$; (d) $\Gamma = 0.06, k = 0.4$.

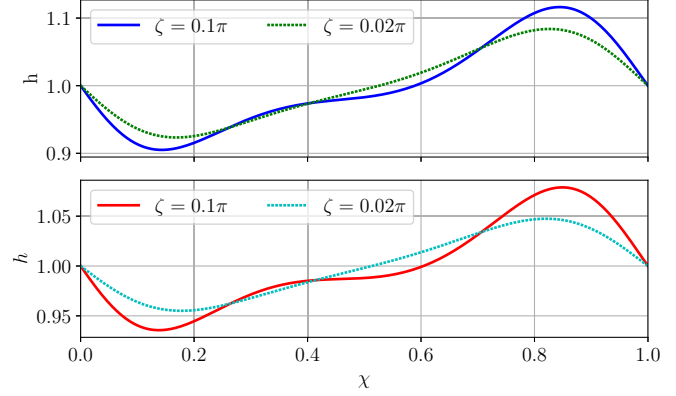


FIG. 15. Periodic stationary solutions of the γ_2 family for different Γ, Re, ζ , and k . Upper graph: $\Gamma = 0.4, \text{Re} = 12, k = 0.5$. Lower graph: $\Gamma = 0.06, \text{Re} = 15, k = 0.4$.

Next, we present the shape of the γ_1 and γ_2 waves for different Γ, ζ , and Re and for a moderate k in Fig. 12. For a fixed set of parameters we can easily see that ζ has a destabilizing effect for both the γ_1 and the γ_2 family. In Fig. 13 we have computed a portrait of the film evolution in the phase plane ($h'-h$). From here we see that the character of the film dynamic is time periodic.

The next three figures, Figs. 14, 15, and 16, are dedicated to understanding well the effects of Re, ζ , and Γ on the flow for the γ_2 wave family. Changing parameter set combinations our results show that, unlike Re, both ζ and Γ have destabilizing effects.

D. Results of the numerical simulation

Figure 17 is dedicated to the long-time simulation of the evolution equation, (52). The various graphs indicate the long-time free surface evolution for different Γ, ζ , and Re. Panel (1, 1) shows final permanent waves over long-term simulation of our model for a Newtonian film over a flat surface ($\Gamma = \zeta = 0$) at an inclination of $\beta = \pi/4$. We have used $\text{Re} = 3.53$ and $\text{We} = 500$ with a time increment $\Delta t = 0.05$. This study shows a good match with the final permanent waveform predicted by Joo *et al.* in their Fig. 7 [55]. Panel (1, 2) shows

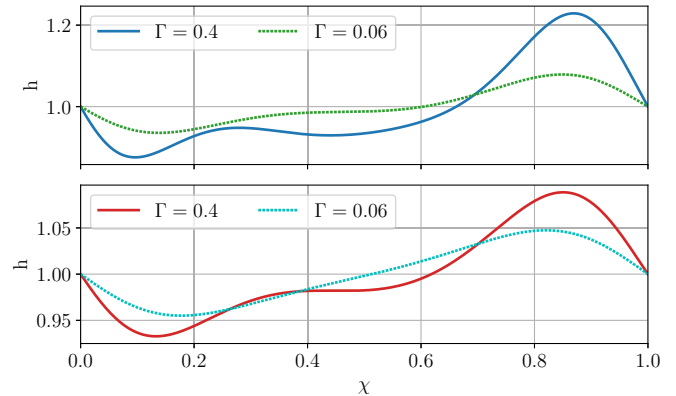
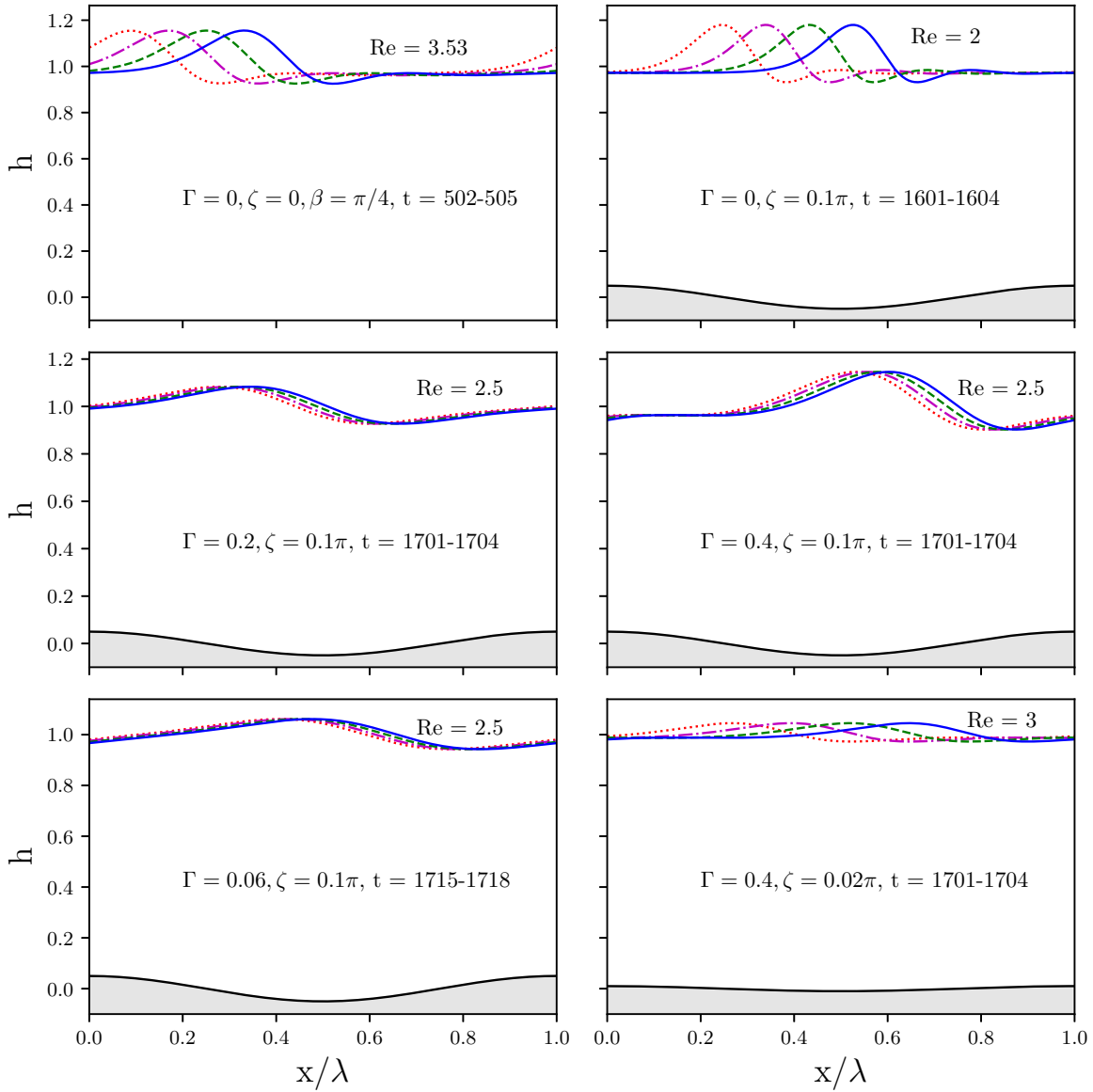


FIG. 16. Periodic stationary solutions of the γ_2 family for different Γ, Re , and ζ . Upper graph: $\zeta = 0.1\pi, \text{Re} = 15, k = 0.4$. Lower graph: $\zeta = 0.02\pi, \text{Re} = 15, k = 0.4$.


 FIG. 17. Free surface configuration for various Γ , ζ , and Re from time-dependent simulations.

the results for a Newtonian film over a wavy bottom. We have chosen $Re = 2$, $We = 400$, $\beta = \pi/3$, and $\Delta t = 0.1$ in order to compare our results with those of Mukhopadhyay and Mukhopadhyay [48] and found a very good match between the two simulations. Panels (2,1), (2,2), and (3, 1) shows final permanent steady waves for $Re = 2.5$, $\beta = \pi/3$, $We = 45000$, $\Delta = 0.05$, and $\zeta = 0.1\pi$ for different Γ values. The amplitude of the disturbances increases as Γ increases. The last panel, (3,2), shows the same result for $\Gamma = 0.4$ and $\zeta = 0.02\pi$ (the rest of the parameters remain the same). Compared with panel (2, 2) we conclude that in the nonlinear regime an increasing ζ increases the amplitude of the disturbances.

X. CONCLUSION

We have investigated the flow of viscoelastic fluid over an undulated periodic bottom with moderate steepness. We have chosen Walters' B'' viscoelastic fluid model for our study, as it requires only one non-Newtonian parameter. This model

represents an approximation to first order in elasticity, i.e., it is valid for short or rapidly fading memory liquids (weakly elastic). Depending upon the relaxation time we have chosen a set of three values, 0.06, 0.2, and 0.4, for the viscoelastic parameter Γ . We performed the entire study primarily for a general periodic bottom profile, then to discuss the results we chose a sinusoidal bottom of moderate steepness. A Benney-type nonlinear evolution equation is derived for long wavelengths considering the effect of waviness of the bottom and the characteristics of the viscoelastic fluid. The linear stability has been analyzed from the spatial and temporal viewpoints. The spatial case is discussed on the basis of Whitham's [47] wave hierarchy.

The weakly nonlinear analysis has been performed with the derivation of a complex Ginzburg-Landau equation using the method of multiple scales. In our study we found both the supercritical stable and the subcritical unstable regions. We have discussed in detail the threshold amplitude and nonlinear wave speed in these two regions.

The results show that the viscoelastic parameter Γ always plays a destabilizing role, while the bottom steepness ζ has a dual effect on the uphill and downhill regions in linear and weakly nonlinear analyses. The physical reason behind this can be analyzed thus: we have taken the wavelength of the sinusoidal bottom as λ . Now, we have considered the uphill portion from $\lambda/2$ to λ , which can be viewed as an inclined plane, and the flow is in disfavor of gravity in this region. As $\zeta \rightarrow 0$, $\theta \rightarrow 0$, which gives $\cos(\beta - \theta)/\sin \beta \rightarrow \cot \beta$ and $\sin(\beta - \theta)/\sin \beta \rightarrow 1$, i.e., we retrieve a flat inclined plane with inclination angle β and we lose the effect of waviness of the bottom. So, in this region an increasing ζ has a stabilizing effect. On the contrary, the downhill portion is from 0 to $\lambda/2$, which can again be viewed as an inclined plane, and the flow is in favor of gravity in this region. Now, as we increase the steepness in the downhill region, $\cos(\beta - \theta) \rightarrow 0$ and $\sin(\beta - \theta) \rightarrow 1$ with $\beta - \theta \rightarrow 90^\circ$ as $\zeta \rightarrow 0.588$, i.e., it behaves like a vertical plane (though it is mathematically true, we geometrically lose the structure of the assumption of waviness). This is the reason that increasing ζ in the downhill portion has a destabilizing effect. Thus to get a perfect reflection of the impact of the steepness parameter ζ on the waviness of the (sinusoidal) bottom profile, we have to restrict ourselves to small values of the parameter ζ , though the theory is valid for moderate steepnesses as well.

Moving forward we have performed a traveling wave solution of the nonlinear evolution equation, (52). By applying a forcing frequency signal at the inlet the traveling waves can be observed in the experiments. These periodic waves remain stationary in a moving frame of reference $\chi = x - ct$, where c is the speed of the frame and hence the speed of the wave. Under this moving reference frame the evolution equation, (52), is recast into a three-dimensional dynamical system. Two wave branches are found, as the family of the slow waves γ_1

and the family of the faster-growing waves γ_2 . Along with the Reynolds number Re , the viscoelastic parameter Γ and the bottom steepness ζ values increase, and all have destabilizing effects by amplifying the wave amplitudes.

Finally, a time-dependent numerical simulation has been performed to solve the evolution equation, (52), with Scikit-FDif. The presence of bottom corrugation and the effect of the fluid property have a good impact on the time-independent waves of permanent form. As stated earlier, Γ and ζ both have destabilizing effects in the nonlinear regime.

Several research works have been performed so far on the topic of viscoelastic fluid flow as well as accounting for the bottom topography using different modeling techniques. However, most of them have studied specific bottom structures. Our study has been performed using a general periodic bottom; also, we have discussed a particular form of the bottom as a case study. We expect that our study will motivate researchers in future to explore these kinds of problems from different aspects and points of view.

DATA AVAILABILITY

The data that support the findings of this study are available from the corresponding author upon request.

ACKNOWLEDGMENTS

The authors express their gratitude to the referees for their attention to the manuscript and valuable comments and suggestions to improve the paper. One of the authors (A.M.) is grateful to Prof. Dr. Andreas Wierschem of Friedrich-Alexander-University of Erlangen-Nürnberg, Erlangen, Germany, for providing related literature in the field.

-
- [1] R. L. Webb, *Principles of Enhanced Heat Transfer* (Wiley, New York, 1994).
 - [2] S. V. Alekseenko, V. E. Nakortiaikov, B. G. Pokusaev, and T. Fukano, *Wave Flow of Liquid Films* (Begell House, Danbury, CT, 1994).
 - [3] A. E. Dukler, The role of waves in two phase flow: Some new understandings, *Chem. Eng. Educ.* **11**, 108 (1977).
 - [4] P. N. Yoshimura, T. Nosoko, and T. Nagata, Enhancement of mass transfer into a falling laminar liquid film by two-dimensional surface waves—Some experimental observations and modeling, *Chem. Eng. Sci.* **51**, 1231 (1996).
 - [5] S. J. Weinstein and K. J. Ruschak, Coating flows, *Annu. Rev. Fluid Mech.* **36**, 29 (2004).
 - [6] P. Kapitza, Wave flow of thin layers of viscous liquid. I. Free flow, *Zh. Eksp. Teor. Fiz.* **18**, 3 (1948).
 - [7] P. Kapitza and S. Kapitza, Wave flow of thin layers of a viscous fluid. III. Experimental study of undulatory flow conditions, *Zh. Eksp. Teor. Fiz.* **19**, 105 (1949).
 - [8] T. B. Benjamin, Wave formation in laminar flow down an inclined plane, *J. Fluid Mech.* **2**, 554 (1957).
 - [9] C.-S. Yih, Stability of liquid flow down an inclined plane, *Phys. Fluids* **6**, 321 (1963).
 - [10] D. J. Benney, Long waves on liquid films, *J. Math. Phys.* **45**, 150 (1966).
 - [11] G. D. Fulford, The flow of liquids in thin films, in *Advances in Chemical Engineering*, edited by T. B. Drew, J. W. Hoopes, T. Vermeulen, and G. R. Cokelet (Academic Press, New York, 1964), Vol. 5, p. 151.
 - [12] T. J. Hanratty, Interfacial instabilities caused by air flow over a thin liquid layer, in *Waves on Fluid Interfaces*, edited by R. E. Meyer (Academic Press, New York, 1983), pp. 221–259.
 - [13] S. P. Lin, and C. Y. Wang, Modelling wavy film flow, in *Encyclopedia of Fluid Mechanics: Vol. 1. Flow Phenomena and Measurement*, edited by N. P. Chermisinoff (Gulf Publishing, Houston, TX, 1985), pp. 931–951.
 - [14] H. Chang, Wave evolution on a falling film, *Annu. Rev. Fluid Mech.* **26**, 103 (1994).
 - [15] H. I. Andersson and E. N. Dahl, Gravity-driven flow of a viscoelastic liquid film along a vertical wall, *J. Phys. D: Appl. Phys.* **32**, 1557 (1999).
 - [16] D. W. Beard and K. Walters, Elastico-viscous boundary-layer flows. I. Two-dimensional flow near a stagnation point, *Math. Proc. Cambr. Philos. Soc.* **60**, 667 (1964).

- [17] A. S. Gupta, Stability of a visco-elastic liquid film flowing down an inclined plane, *J. Fluid Mech.* **28**, 17 (1967).
- [18] W. Lai, Stability of an elastico-viscous liquid film flowing down an inclined plane, *Phys. Fluids* **10**, 844 (1967).
- [19] A. S. Gupta and L. Rai, Note on the stability of a visco-elastic liquid film flowing down an inclined plane, *J. Fluid Mech.* **33**, 87 (1968).
- [20] B. S. Dandapat and A. S. Gupta, Long waves on a layer of a visco-elastic fluid down an inclined plane, *Rheol Acta* **17**, 492 (1978).
- [21] E. S. G. Shaqfeh, R. G. Larson, and G. H. Fredrickson, The stability of gravity driven viscoelastic film-flow at low to moderate Reynolds number, *J. Non-Newton. Fluid Mech.* **31**, 87 (1989).
- [22] F. Kang and K. P. Chen, Nonlinear elastic instability of gravity-driven flow of a thin viscoelastic film down an inclined plane, *J. Non-Newton. Fluid Mech.* **57**, 243 (1995).
- [23] B. S. Dandapat and A. S. Gupta, Solitary waves on the surface of a viscoelastic fluid running down an inclined plane, *Rheol Acta* **36**, 135 (1997).
- [24] P.-J. Cheng, H.-Y. Lai, and C.-K. Chen, Stability analysis of thin viscoelastic liquid film flowing down on a vertical wall, *J. Phys. D: Appl. Phys.* **33**, 1674 (2000).
- [25] B. Uma and R. Usha, Dynamics of a thin viscoelastic film on an inclined plane, *Int. J. Eng. Sci.* **44**, 1449 (2006).
- [26] H. Tougou, Long waves on a film flow of a viscous fluid down an inclined uneven wall, *J. Phys. Soc. Jpn.* **44**, 1014 (1978).
- [27] C. Pozrikidis, The flow of a liquid film along a periodic wall, *J. Fluid Mech.* **188**, 275 (1988).
- [28] A. Wierschem, C. Lepski, and N. Aksel, Effect of long undulated bottoms on thin gravity-driven films, *Acta Mech.* **179**, 41 (2005).
- [29] Y. Y. Trifonov, Stability and nonlinear wavy regimes in downward film flows on a corrugated surface, *J. Appl. Mech.: Tech. Phys.* **48**, 91 (2007).
- [30] Y. Y. Trifonov, Stability of a viscous liquid film flowing down a periodic surface, *Int. J. Multiphase Flow* **33**, 1186 (2007).
- [31] E. Mogilevskiy and V. Shkadov, Stability of a thin film flow on a weakly wavy wall, *Int. J. Multiphase Flow* **114**, 168 (2019).
- [32] S. Veremieiev and D. H. Wacks, Modelling gravity-driven film flow on inclined corrugated substrate using a high fidelity weighted residual integral boundary-layer method, *Phys. Fluids*, **31**, 022101 (2019).
- [33] C. Ruyer-Quil and P. Manneville, Improved modeling of flows down inclined planes, *Eur. Phys. J. B* **15**, 357 (2000).
- [34] S. J. D. D'Alessio, J. P. Pascal, and H. A. Jasmine, Instability in gravity-driven flow over uneven surfaces, *Phys. Fluids* **21**, 062105 (2009).
- [35] M. Vlachogiannis and V. Bontozoglou, Experiments on laminar film flow along a periodic wall, *J. Fluid Mech.* **457**, 133 (2002).
- [36] A. Wierschem and N. Aksel, Instability of a liquid film flowing down an inclined wavy plane, *Physica D: Nonlin. Phenom.* **186**, 221 (2003).
- [37] A. Wierschem, M. Scholle, and N. Aksel, Vortices in film flow over strongly undulated bottom profiles at low Reynolds numbers, *Phys. Fluids* **15**, 426 (2003).
- [38] L. A. Dávalos-Orozco, Instabilities of thin films flowing down flat and smoothly deformed walls, *Micrograv. Sci. Technol.* **20**, 225 (2008).
- [39] T. Häcker and H. Uecker, An integral boundary layer equation for film flow over inclined wavy bottoms, *Phys. Fluids* **21**, 092105 (2009).
- [40] C. Heining and N. Aksel, Bottom reconstruction in thin-film flow over topography: Steady solution and linear stability, *Phys. Fluids* **21**, 083605 (2009).
- [41] T. Pollak and N. Aksel, Crucial flow stabilization and multiple instability branches of gravity-driven films over topography, *Phys. Fluids* **25**, 024103 (2013).
- [42] Y. Trifonov, Nonlinear waves on a liquid film falling down an inclined corrugated surface, *Phys. Fluids*, **29**, 054104 (2017).
- [43] N. Aksel and M. Schörner, Films over topography: From creeping flow to linear stability, theory, and experiments, a review, *Acta Mech.* **229**, 1453 (2018).
- [44] C. Heining and N. Aksel, Effects of inertia and surface tension on a power-law fluid flowing down a wavy incline, *Int. J. Multiphase Flow* **36**, 847 (2010).
- [45] A. Wierschem, V. Bontozoglou, C. Heining, H. Uecker, and N. Aksel, Linear resonance in viscous films on inclined wavy planes, *Int. J. Multiphase Flow* **34**, 580 (2008).
- [46] C. Heining, V. Bontozoglou, N. Aksel, and A. Wierschem, Nonlinear resonance in viscous films on inclined wavy planes, *Int. J. Multiphase Flow* **35**, 78 (2009).
- [47] G. B. Whitham, *Linear and Nonlinear Waves. Pure and Applied Mathematics* (Wiley, New York, 1974).
- [48] S. Mukhopadhyay and A. Mukhopadhyay, Hydrodynamics and instabilities of falling liquid film over a non-uniformly heated inclined wavy bottom, *Phys. Fluids* **32**, 074103 (2020).
- [49] E. J. Doedel, A. R. Champneys, T. F. Fairgrieve, Y. A. Kuznetsov, B. Sandstede, and X. Wang, *AUTO 97: Continuation and Bifurcation Software for Ordinary Differential Equations (with HomCont)* (Concordia University, Montreal, Canada, 2008).
- [50] A. Mukhopadhyay and A. Mukhopadhyay, Nonlinear stability of viscous film flowing down an inclined plane with linear temperature variation, *J. Phys. D: Appl. Phys.* **40**, 5683 (2007).
- [51] A. Mukhopadhyay and A. Mukhopadhyay, Stability of conducting viscous film flowing down an inclined plane with linear temperature variation in the presence of a uniform normal electric field, *Int. J. Heat Mass Transf.* **52**, 709 (2009).
- [52] A. Mukhopadhyay and S. Haldar, Long-wave instabilities of viscoelastic fluid film flowing down an inclined plane with linear temperature variation, *Z. Naturforsch. A* **65**, 618 (2010).
- [53] S. P. Lin and M. V. G. Krishna, Stability of a liquid film with respect to initially finite three-dimensional disturbances, *Phys. Fluids* **20**, 2005 (1977).
- [54] N. Cellier and C. Ruyer-Quil, Scikit-finite-diff, a new tool for PDE solving, *J. Open Source Software* **4**, 1356 (2019).
- [55] S. W. Joo, S. H. Davis, and S. G. Bankoff, Long-wave instabilities of heated falling films: Two-dimensional theory of uniform layers, *J. Fluid Mech.* **230**, 117 (1991).
- [56] B. Scheid, C. Ruyer-Quil, U. Thiele, O. A. Kabov, J. C. Legros, and P. Colinet, Validity domain of the Benney equation including the Marangoni effect for closed and open flows, *J. Fluid Mech.* **527**, 303 (2005).
- [57] H.-C. Chang, E. A. Demekhin, and D. I. Kopelevich, Nonlinear evolution of waves on a vertically falling film, *J. Fluid Mech.* **250**, 433 (1993).